Optimising Process Parameters for Fabricating AA4047 multi-layer wall by Cold Metal Transfer based Wire Arc Additive Manufacturing (CMT-WAAM) and studying its Mechanical Properties

A DISSERTATION

SUBMITTED IN PARTIAL FULFILLMENT OF THE REQUIREMENTS FOR THE AWARD OF THE DEGREE

OF

MASTER OF TECHNOLOGY

IN

PRODUCTION ENGINEERING

Submitted by

Archana Gopal

2K21/PRD/02

Under the supervision of

Dr. N. Yuvraj

Assistant Professor

Mechanical Engineering Department

DEPARTMENT OF MECHANICAL ENGINEERING

DELHI TECHNOLOGICAL UNIVERSITY

(Formerly Delhi College of Engineering)

Bawana Road, Delhi-110042

MAY, 2023

CANDIDATE'S DECLARATION

I, **Archana Gopal**, Roll No. **2K21/PRD/02** of M.Tech (Production Engineering), hereby certify that the project Dissertation titled "**Optimising Process Parameters for Fabricating AA4047 multi-layer wall by Cold Metal Transfer based Wire Arc Additive Manufacturing (CMT-WAAM) and studying its Mechanical Properties"** which is submitted by me to the Department of Mechanical Engineering, Delhi Technological University, Delhi in partial fulfilment of the requirement for the award of the degree of the Master of Technology, is original and not copied from any source without proper citation. This work has not previously formed the basis for the award of any Degree, Diploma Associateship, Fellowship or other similar title or recognition.

Place: Delhi

Date:

Archana Gopal

2K21/PRD/02

M.Tech (Production Engineering)

Delhi Technological University

CERTIFICATE

I hereby certify that the Project Dissertation titled **"Optimising Process Parameters for Fabricating AA4047 multi-layer wall by Cold Metal Transfer based Wire Arc Additive manufacturing (CMT-WAAM) and studying its Mechanical Properties"** which is submitted by **ARCHANA GOPAL**, 2K21/PRD/02, Mechanical Engineering Department, Delhi Technological University, Delhi inpartial fulfilment of the requirement for the award of the degree of Master of Technology, is arecord project work carried out by the student under my supervision. To the best of my knowledge this work has not been submitted in part or full for any Degree or Diploma to this University or elsewhere.

Place: Delhi

Date:

Dr. N. Yuvraj

SUPERVISOR

Assistant Professor

Department of Mechanical Engineering

Delhi Technological University

ABSTRACT

This paper aims to fabricate multilayer wall of AA4047 by Wire Arc Additive Manufacturing (WAAM) through Cold Metal Transfer (CMT). To determine the optimal process parameters, optimization of monolayer parameters is carried out via Response Surface Methodology (RSM) – Analysis of Variance (ANOVA). There is an overall impact on the operational characteristics of fabrication time, and heat input (HI); geometrical characteristics of wall height, and width; and metallurgical characteristics of strength, microhardness, porosity, and microstructure for the deposited layers.

The multilayer wall had average Microhardness of 49.90 HV, Yield Strength of 67.5 MPa, Elastic Modulus of 1032.58 MPa, Percentage Elongation (PE) of 31.3, and Ultimate Tensile Strength (UTS) of 146.5615 MPa. It was concluded that UTS, and microhardness increased, and deposition rate, PE and pore size decreased, as HI was decreased by decreasing current and increasing travel speed, on increasing the number of layers.

KEYWORDS: WAAM, CMT, AA4047, Heat Input, Tensile Strength, Hardness

ACKNOWLEDGEMENT

First of all, I wish to convey my deep gratitude and sincere thanks to my M.Tech supervisor, Dr N. Yuvraj for giving me an opportunity to pursue this research work at Delhi Technological University. I feel very fortunate that I got an opportunity to work under his supervision. I would like that thank all the staff and faculty members of Mechanical Engineering Department for their continuous help, encouragement and support.

ARCHANA GOPAL

2K21/PRD/02

M.Tech (Production Engineering)

Delhi Technological University

TABLE OF CONTENTS

LIST OF FIGURES

LIST OF TABLES

LIST OF ABBREVIATIONS

Additive Manufacturing	AM
Cold Metal Transfer	CMT
Wire Arc Additive Manufacturing	WAAM
Binder jetting	BJ
Material Extrusion	ME
Direct energy deposition	DED
Powder bed fusion	PBF
Fused deposition modelling	FDM
Tungsten Inert Gas	TIG
Metal Inert Gas	MIG
Plasma Arc Welding	PAW
Heat Affected Zone	HAZ
Travel Speed	TS
Ultimate Tensile Strength	UTS
Response Surface Methodology	RSM
Nozzle Tip Distance	NTD
Universal Testing Machine	UTM
Electric Discharge Machining	EDM
Design of Experiment	DOE
Face Centered Composite Design	FCCD
Heat Input	HI
Hydrogen fluoride	HF
Hydro Chloric Acid	HCl
Water	H_2O
Analysis of variance	ANOVA
Near Immersion Active Cooling	NIAC
Interlayer Temperature	IT
Sum of Squares	SS
Mean Square	MS
Signal to noise ratio	S/N
Percentage Dilution	PD

CHAPTER 1 INTRODUCTION

1.1 ADDITIVE MANUFACTURING (AM)

Ere the industrial revolutions, livelihood was subjected to craftsmanship and agriculture. With time the urge to develop newer materials and manufacturing processes came up and people wanted to use better quality products and enhance their lifestyle. This started research for newer materials and fabrication methods, which could be more effective and fast compared to the traditional ones. This trend made the country's economy dependent on its industrial growth via large-scale production and mechanized tooling.

Four stages in the industrial revolution are seen as (a) Stage 1: A shift in manufacturing from manual to the steam-driven, which continued up to 1835, (b) Stage 2: Vast-scale manufacturing by high-end energy resource development, which continued up to 1945, (c) Stage 3: Shift from mechanically driven era to a technology-driven era of Computer, Digital data, and Internet, it continued up to 2015, (d) Stage 4: Integrates advanced manufacturing processes especially Additive Manufacturing(AM) with the Simulation and Optimization, Big data, Internet of Things, Augmented Reality, Robotics and AI to create computer-aided manufacturing systems which not only interpret but also use data by Machine Learning to manage numerous intelligent movements back in real-world pacing towards complete automation [1].

Hence the industry is benefited from the flexible product modification, product development, market entrance, reduced cost, and operational unification achieved [2]. The six primary steps of AM are (a) building a 3D model via Software packages, (b) tessellating, (c) stacking, (d) configuring and calibrating the machine, (e) producing prototypes, and (f) post-processing and strength analysis.

As new technologies and techniques for fabrication are developed, design and production research is redefining the boundary of conventional methods. Earlier termed as rapid prototyping (in the 1980s), this process faced advancements and is now termed as Additive manufacturing. Feedstock is used, which is in the form of a powder or wire. It may be fused, heated, or build as stacks by multi-dimensional computer-aided process planning and manufacturing system.

With minimum homo sapiens interaction, it eliminates all needs to remove or mould material further into the shape of a product [3]. Additive manufacturing (AM) is the formal industrial nomenclature, but 3D printing is recognised frequently common alternative, owing to a joint effort by the ASTM-American Society for Testing and Materials with ISO-International Standards Organization [4].

Due to its capacity to create complicated geometries, decrease waste, increase design flexibility, and lower the cost of customization, metallic 3-d printing (AM) is among the most key techniques employed in the manufacturing business [5,6]. For example, some titanium surgical implants have

recently been printed using it. Boeing 777 with engine GE9X uses a heat exchanger system, consisting of 300 individual pieces. Owing to AM evolution, it just requires one, which also happens to be 25% cheaper and 40% lighter.

SpaceX has used MAM components to cut down on production time and weight for its Super Draco and Raptor engines, and NASA plans to do the same for the Space Shuttle's primary engine in the near future. Made of 308LSi austenitic stainless steel, the world's 1st additively manufactured metallic bridge is at De Wallen, Amsterdam, it stretches 10.50 meters over the Oudezijds Achterburgwal canal. [7-9]

1.1.1 Types of Additive Manufacturing

Binder jetting (BJ), Sheet Lamination, Material Extrusion (ME), Direct energy deposition (DED), Vat Polymerization, and Powder bed fusion (PBF) are the six main types of MAM processes defined by ASTM/ISO 52900:2017, others are Friction Stir Additive Manufacturing, WAAM as shown in Fig. 1.1.1 [4]. Metals are involved in just four of these six processes. Acknowledging advancements in AM, metal, polymer, ceramic, composite, and bio-compatible materials are just a few examples that can be used [10].

Binder Jetting results are analogous to those of printing text on paper. When metal powdered granules bond to one another through a liquid binder, it creates a solid material layer. This printing process normally takes place at room temperature, this assists in avoiding thermally induced errors such as undesired grain development and distortion which are common in other MAM techniques that rely on a heat source [11-14]. The base material also acts as a substitute support structure while the permanent one is being built. Waste is reduced since there is no need for framing [15-17].

DED- Direct Energy Deposition is a method that, like welding, employs a concentrated heat source to melt materials that are placed via a nozzle [18]. It accounts for 16% of the overall MAM market and is mostly used for producing fairly close parts and fixing or making improvements to existing parts [19,20]. The DED method makes use of a heat source that may melt a feedstock (wire and powder) to a liquid state [21,22].

It is touted as being more efficient than competing technologies since it doesn't need the use of powerful lasers. In addition to being more cost-effective than PBF (Powder Bed Fusion) by 60-80%, it is simpler to run too. Fused deposition modelling (FDM) was developed for additive production of polymeric as well as composite layers [21-24].

The bound powder and ceramic release substance, are held on separate spools in a sealed container, and extruded by a conventional Material Extrusion machine. When using polymer binders, the 3d printer must raise the temperature of the feed higher than its melting point [25-28]. When using an

electron or laser beam, PBF melts the material, allowing for the deposition of several coatings of material at once.

Metal direct laser sintering is being used to create bigger mechanical components like turbine blades, it has the potential of creating thick multi-layered substances but has a massive operational expense. PBF falls into a similar category.

Similarly, electron beam melting necessitates a vacuum during the production of functional components, whereas selective laser heating has higher operating costs than the aforementioned AM techniques [29-33].

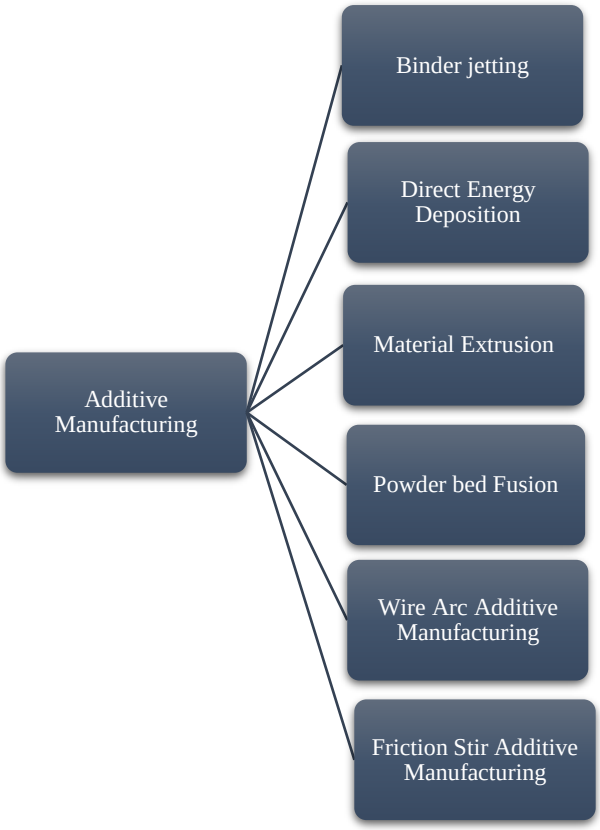

Fig.1.1.1 Types of Additive Manufacturing

1.1.2 Limitations of AM

Calvert et. al declared that elevated temperatures and gradients developed in electron beam welding caused accelerated grain growth, a decrease in isotropic behaviour, a decrement in levels of stress dilution, and other typical cast defects. They also explained that it required some machining within every succeeding layer for a better connection surface [36].

The traditional subtractive production process for fabrication involved around 85 percent wastage of base material. The AM process requires lesser material bulk volume and concurrently improves the

strength-to-weight ratio. Some of its latest techniques that are extensively used are selective laser sintering, cold spray AM, electron beam welding, layered friction stir AM [37]

Sing et al. [38] declared that selective laser melting fabricated components with remarkable defects along with porosity. Mertens et al. [39] observed that the enormous laser energies utilised in laser beam AM would lead to more material loss due to evaporation, unnecessary spatter, and degradation of exterior nature by baling.

SMD (shape metal deposition) has an extensive build rate but inferior surface quality and bad dimensional tolerance, this issue was resolved by the application of LBAM. The parts made had better properties but had a tremendous cost of operation, slow build rates, and moderate bulk volume.

Hang et al. stated that making metal parts by AM got commonly restrained to fusion-based methods where the powder substrates have to be heated above the melting point and, as the laser or beam moves forward, the consequent molten metal pool tempers down, getting solidified according to the scanning tool path followed by the laser or beam [40].

Like in fusion welding and casting, fusion-based MAM unavoidably negotiates in quality control of the material; cooled material suffers from hot cracking (especially in pure aluminium), porosity (especially in LBAM-made parts), residual stresses, and other defects.

These defects get elevated due to the improper grain structure formed by the swift cooling rate and a sharp temperature gradient. Even after years of research, the quality of fusion-based components still lacks.

Even in Cold Spray AM, which is the most researched AM in recent times, FSP has to be followed after deposition due to the porosity, micro-cracks, and improper bindings in some places. Thus, there has to be post-processing done on FSP machines, this increases the cost of the component as it undergoes two different exclusive machine setups. These limitations cause the emergence of Wire Arc Additive Manufacturing (WAAM).

1.2 WIRE ARC ADDITIVE MANUFACTURING (WAAM)

The technique of Wire Arc Additive Manufacturing (WAAM) for aluminum alloy has evolved swiftly in previous years [41]. WAAM is a continuous feed technique that employs an arc to be the heat source while the metallic wire is the feedstock [42]. In contrast to the low energy efficiency of additive manufacturing (AM) using electron beams and laser energies, the energy efficiency in WAAM may reach as high as 90 percent [43,44].

Feedstock transfer efficiency can go up to 100 percent [45]. This gives high material efficiency and makes the process economical. It has a high formation rate of approximately 10 kg/hr [46]. The WAAM Ti-6Al-4V alloy's fatigue life exceeded that of the cast sample, indicating its suitability for

superior strength applications [47]. It is best for sizable components with a moderate degree of geometrical intricacy [48,49].

If process parameters are not chosen wisely, they can result in high porosity, inferior mechanical properties, and collapse, initiated by critical heat deposition [50,51]. One of the crucial parameters for WAAM is heat input [52-54]. A lot of researchers have analyzed the effect of heat input in WAAM [55-58].

WAAM owns its existence to Direct Energy Deposition (DED). DED is a technique that, like welding, uses an intensified heat source to melt solids that are deposited through a nozzle [59]. According to Tepylo, Vafadar, it accounts for 16% of the total AM industry and is ideal for manufacturing relatively near components and repairing or enhancing pre-existing ones [60,61].

The DED technique employs a thermal source that can transform a feedstock (wire or granules) into a liquid state [62,63]. It is expected to account for a market share of approximately 80% of the revenue generated by AM. Furthermore, it is 60-80% less expensive than PBF (Powder Bed Fusion), and it is also easier to operate [63].

Powder-fusing systems are optimal for tiny, complicated sections with detailed and difficult features, whereas wire-fusing systems with DED technology typically have higher rates of deposition but lower quality of finish. Wire or powder can be used as feed; there both have advantages as well as disadvantages. When using powder as feed, a certain quantity of additives can be used to enhance the properties of the deposited material, so a variety of powder mixtures can be formed, deposited, and analyzed, making the process flexible.

Along with an increase in the variability of the powder, there comes a risk of impurity embrittlement. When using solid rods as feed, the ease of variability decreases but the risk of impurity embrittlement diminishes, allowing the formation of high-quality deposited material [64].

1.3 HEAT SOURCES IN WAAM

On understanding the effect of heat input value on the properties of WAAM-made products, it is critical to know about the various heat sources that can be employed in WAAM. These are Tungsten Inert Gas (TIG), Metal Inert Gas (MIG), and Plasma Arc Welding (PAW) [65-69].

Although PAW has more focussed heat than MIG, PAW has the limitation of high gas usage and costly machinery [69-71]. The arc welding source creates heat energy, that widens the heat-affected zone (HAZ). On comparing with wrought alloys, these have poor build quality. Aluminum alloys have a large linear expansion leading to solidification cracking [72-75].

The MIG process is extensively used for aluminium alloys, but can lead to intense solidification cracking and critical deformation [76,77]. By decreasing heat input in the MIG plasma hybrid process

of AA 7075, the solidification cracking tendency is reduced [78,79]. For AA 6061 alloy, increasing the wire feed speed, initially increased the tendency of solidification cracking and later decreased it [80]. A test of transverse motion weldability depicts the solidification cracking tendency of AA 7075 alloy when compared between CMT and MIG processes [81].

1.4 COLD METAL TRANSFER

The MIG process has revolutionized into (CMT) process, seeking the advantages of lower heat input, lower residual stress, more stable arc, higher controllability of material deposition, and diminished spatter [82-84]. Fronius company played a huge part in evolving the CMT technique. The wire feed was incorporated into the welding procedure. They programmed the complete control of the system robotically.

For each short circuit that occurred, the robotic control interrupted the power cycle. The CMT cycle for material deposition has three phases- the peak current phase, the background current phase, and the short-circuiting phase [85,86]. In the first phase, high current and constant voltage cause the lightening of the arc, heating the feed wire to initiate the droplet. In the second phase, the current is lowered to stop the transfer of droplets formed [87,88].

The voltage is decreased to zero in the short circuit stage. A system of oscillatory wire feeders having an approximate frequency of less than 70 Hz, retracts the wire against the work surface [89]. This decreases the heat input, reducing deformation [90]. It is in this phase that the heat is received by the wire from the weld pool by the intermediate droplet [91]. Hence, spatter and heat input gets reduced. In this paper, a CMT technology for getting high deposition rates by WAAM is proposed.

CHAPTER 2 LITERATURE REVIEW AND OBJECTIVES OF PRESENT WORK

2.1 LITERARTURE REVIEW

2.1.1 WAAM

Su et al. [92] analyzed the effect of source energy on the mechanical and microstructural properties of the Al-Mg alloy manufactured using WAAM. Various levels of heat energy were generated by altering the transverse speed and the wire feed speed to produce numerous Al-Mg parts. Significant columnar grains within the interlayer and interior layers got transformed into fine equiaxed grains by modifying the heat input [93].

Wang et al. [94] displayed grain refinement and porosity decrement in components with thin walls by modifying the current and the pulse frequency. At reduced current values and pulse rates, finer grains and uniform microstructure were developed as a result of the quick cooling of the material [95].

Guo et al. worked on Al-Si alloy thin wall components and concluded that WAAM performed better than casting. To increase the controllability of the process, the travel speed (TS) was increased by decreasing heat input levels [96,97]. Zhou et al. concluded that to minimize the diameter of the equiaxed grain and to lower the volume fraction, heat input was lowered, incrementing formation rates and cooling rates [98].

2.1.2 CMT

The tendency of solidification cracking is diminished by CMT due to its low heat input characteristic [59,60]. This characteristic also reduces intermediate layer thickness, improving joint efficiency [99]. CMT, also shows lowered dilution cladding [100].

Robotically governed CMT gives improved process efficiency, travel speed, flexibility, part strength, and 100% material efficiency [101-103]. It has a variety of applications in aeronautics, structures, electronic parts, and locomotive media [104,105]. CMT has a variety of arc modes, namely advanced CMT, pulse CMT, and pulse advanced CMT [106].

Cong analyzed the CMT technique with variable polarity technique. It effectively eradicated porosity and showed that the most important variables were minimal heat input, a refined equiaxed grain arrangement, and efficient oxide cleansing of the feed wire. In terms of eradicating porosity, the CMT technique with variable polarity mode is more practical compared to the arc modes. This arc mode has increased application potential in WAAM [107].

Thin-walled Al-6Mg components with a uniform structure and low porosity were manufactured via WAAM utilizing a CMT-VP arc energy source with multiple arc modes. Components made had (Ultimate Tensile Strength) UTS, greater than those of other mode components and also, better than the wrought metal. It is capable of converting columnar grains into equiaxed grains, refining the grains, and enhancing mechanical performance [108].

2.1.3 Fabricating Aluminium Alloys

In the past few years, numerous scientists and researchers have been trying to produce a variety of aluminium alloys, like Al-Mg, Al-Cu, and Al-Si alloys via the WAAM technique [109]. Due to the exceptionally high strength of WAAM-made Al-Zn-Mg-Cu aluminium alloy components, many scientists are concentrating on their viability [110].

Alloy was made with the GTAW technique by simultaneously injecting ER2319, Zn, and ER5356 infill wires into the pool of molten metal. When greater than forty layers had been added, liquation splits appeared 50 mm from the base. As the deposition height increased, the internal tension increased, leading to the formation of macro cracks [111].

In a study by Yu et al., the microstructure lacked equiaxed grains and consisted of columnar grains. Defects of cracks and porosity were seen, with a tensile strength of 240 Mpa [112]. Including several wires as feed, leads to improper composition and varied microstructure. The produced parts are highly prone to hot cracking, and their physical characteristics may get degraded [113,114]. Thus, for studying WAAM on unexplored aluminium alloy feed wires, simultaneously combining different feed wires isn't recommended.

Simply employing industrial or readymade aluminium alloy filaments as feed, is a viable option for avoiding the above-mentioned shortcomings in WAAM for aluminium alloys [115]. AA 4047 shows good mechanical characteristics and applications, and is thus, used with TIG joining process [116-119], Laser beam joining process [120,121], Laser Brazing process [122], and CMT Welding process [123]. AA 4047 has applications of layering in aerospace, automotive, and electronic industries, due to its good corrosion resistance, resistance to crack, and ability to bear high temperatures.

2.1.4 CMT-WAAM for Wall Fabrication

Ortega et al. made multilayer AA 4043 deposits via the CMT WAAM route. They first studied monolayer deposits and then worked on the wall formation [124]. V Shukla et al. studied the tensile properties and microstructure of the ER706-6 wall. Before going for the study of the multilayer deposit, they first studied the single-layer deposit [125].

Zhou et. al. [126] stated that sample morphologies of mono-layer Ti6Al4V deposits, need to be evaluated for making multilayer deposits. The bead's morphology was determined by its width, aspect

ratio, and reinforcement. The aspect ratio was defined as the ratio between the width of the bead and the thickness of the reinforcement. The upper portion of the made layer was thin and slanted, making succeeding layers difficult to deposit. The succeeding deposition layer's molten pool spilled, causing collapsed faults. The molten pool's spreadability altered multi-layer deposition sample morphology in the CMT-WAAM process [126]. The forming effect improved when each layer's arc beginning point matched the preceding layer's endpoint.

Qi et.al. [127] investigated the effect of process variables of the CMT-WAAM process on the shape and appearance of mono-layer and multi-layer deposits (30 layers) of ER2209 duplex stainless steel. Microstructure was monitored simultaneously with the Process parameters. Monolayer deposits required 60~70 mm/s wire feed speed and 5~7 mm TS. Multi-layer deposits require homogeneous reciprocating additive route formation, 65~75 mm/s wire speed, 7 mm scanning speed, and 60 s interlayer cooling period.

There lies a need for optimization to find a suitable combination of process parameters, like Multi response optimization for WAAM-CMT for SS308L [128], Multi response mathematical modeling of AA6061 weld bead configuration using Response surface methodology (RSM) [129], Multi-response mathematical modeling in CMT welding using RSM- Grey Relational Analysis [130].

Heat is built as the number of deposition layers increases, causing the molten pool to overflow [131]. Therefore, as the number of deposition layers increases current is decreased [132] and the travel speed is increased [133] to get the same effective wall width. In this paper, the current is decreased by increasing the height of the wall.

2.2 RESEARCH GAP

The research gap has been found out by carrying out Literature Review.

CMT-WAAM with AA4047 feed wire, has been less explored. AA 4047 has applications of layering in aerospace, automotive, and electronic industries, due to its good corrosion resistance, resistance to crack, and ability to bear high temperatures.

For making multilayer deposits, initially bead on plate study for finding out the optimised parameters is required, which has been missing in some studies.

The effect of CMT-WAAM process parameters, on heat input, and various mechanical properties has not been studied fully.

2.3 OBJECTIVES

The research objectives have been formulated, by understanding the research gap.

To study the weld on bead by CMT-WAAM, with AA 4047 filler wire and AA 6082 substrate, and to study the heat input, percentage dilution, and microhardness of the monolayers with varying current and travel speeds.

To optimise the process parameters (current and travel speed) by analysing the responses of percentage dilution and microhardness of monolayer by Response Surface Methodology (RSM) and Analysis of Variance (ANOVA).

To fabricate a multilayer wall, via cold metal transfer (CMT) mode of wire arc additive manufacturing (WAAM), and to study the samples cut out from the various zones of the build wall, for Tensile test, Hardness test, and Microstructural study.

CHAPTER 3 METHODOLOGY

3.1 MATERIAL SELECTION

AA 4043 has been used with the CMT-WAAM process in earlier studies, but AA 4047 has not been studied with the CMT-WAAM technique. AA 4047 has a higher silicon content of about 12%, this helps in minimizing the shrinkage, getting a smooth finish, and improving its fluidity. It has a melting point higher than that of AA 4043, giving it higher resistance to cracking. It can bear high temperatures, has good corrosion and wear resistance, and can bind and shield other metals, making it apt for automotive, and aerospace applications.

The use of AA 4047 filler wire has been done in limited studies. The scope of studying the usage of AA 4047 with the CMT WAAM process has not been yet explored. Thus, more research is needed in this field. AA 4047 feed wire, with 1.2 mm diameter is used. It weighs about 3.5 grams per meter of wire. The AA6082 base plate is 5 mm thick, 100 mm in length, and 60 mm in width, as shown in Fig. 3.1. It is found that AA4047 is compatible with AA4047 for getting proper bindings. The composition of AA4047 filler wire and substrate of AA6082 can be seen as described in Table 3.1.1 [130,134].

Table 3.1.1 Composition of AA4047 and AA6082

Elements (wt. %)	Si	Cr	Cu	Fe	Mg	Mn	Zn	Ti	Be	Al
AA4047	11.85	-	0.02	0.24	0.01.	0.01	0.09	0.01	.0003	Balance
AA6082	1.2	0.25	0.09	0.49	0.58	0.4	.19	-	-	Balance

Fig. 3.1.1 AA6082 Base Plates

3.2 EXPERIMENTAL SET-UP

CMT machine TPS400i made by Fronius is used to carry out the experiments. On working with the automatic mode in CMT-WAAM mode, for every filler wire material, pre-setting is created within the Fronius system after years of research on the behavior of the material. The process parameters of the voltage, current, and wire feed rate are interdependent on each other.

Hence, on changing any one parameter, the other two are controlled automatically due to the smart, Industry 4.0 enabled CMT set up by Fronius Austria Ltd, as shown in Fig. 3.2.1. Consequently, the requirement is to select just a single process variable amongst voltage, wire feed rate, and current of which current is selected based on a test run and by the literature review. In addition to that, the most essential process variable is welding speed, as demonstrated based by the test run and the literature review.

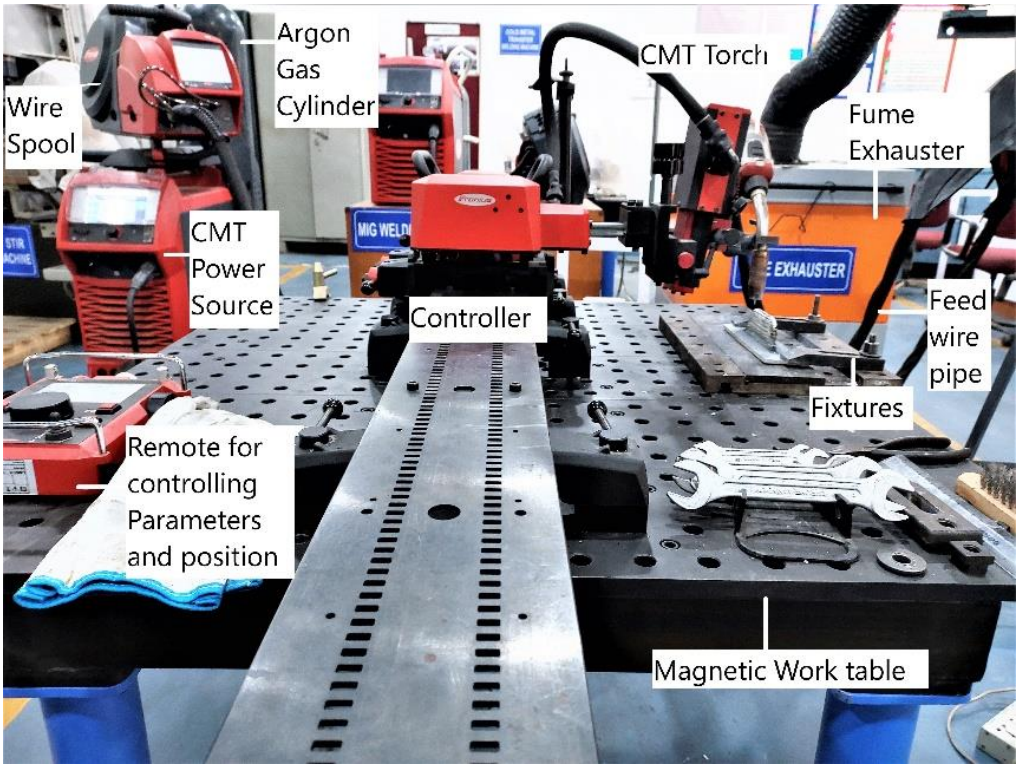

Fig. 3.2.1 Experimental Set-up for CMT-WAAM

Fig. 3.2.2 CMT Power Source, Wire Pool, and Argon Gas cylinder

Fig. 3.2.3 CMT Torch, with Nozzle

Pure argon (99.999%) was used for shielding the molten AA4047 to avoid oxidation and other defects. The gas flow rate influences its cooling rate, leading to an alteration in the specimen's solidification rate. In this work, it is kept constant, at 15 L/min. Before commencing the metal deposition procedure, the substrate was meticulously cleansed with an alkaline solution to clean oil stains and then with acetone ($(CH3)_2CO$).

Fig. 3.2.4 Motion Controller on Work table

Fig. 3.2.5 Remote for controlling robotic motions and process parameters

CMT machine is made up of various parts,

- CMT Power Source, as shown in Fig. 3.2.2
- Wire Spool, as shown in Fig. 3.2.2
- Argon Gas cylinder, as shown in Fig. 3.2.2
- CMT Torch, with Nozzle, as shown in Fig. 3.2.3
- Motion Controller on Work Table, as shown in Fig. 3.2.4
- Remote for controlling robotic motions and process parameters, as shown in Fig. 3.2.5
- Height Adjuster fitted between motion controller and CMT Torch, as shown in Fig. 3.2.6
- Fume Exhauster, for sucking harmful gases released during deposition, as shown in Fig. 3.2.7

Following the cleaning of the AA6082 substrate surface, the base plate was fastened with the help of fixtures, keeping the torch angle at 90 °, 10 mm of nozzle tip distance (NTD), and stick-out at 5 mm. A torch traveler with rectilinear motion is fitted on a gantry robot allowing it to move linearly along three axes to maintain the position of the CMT torch. In this research, among the different parameters, current and welding speed, are chosen due to their extensive impact on the mechanical properties of the made parts.

Fig. 3.2.6 Height Adjuster fitted between motion controller and CMT Torch

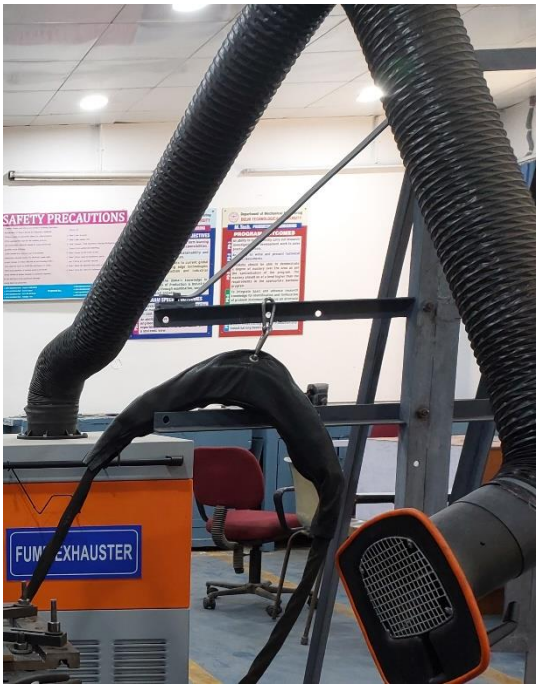

Fig. 3.2.7 Fume Exhauster

3.3 TEST SET-UP

3.3.1 Macro Imaging

Macro images were taken through Trinocular stereo zoom microscope with digital camera as shown in Fig. 3.3.1.1 and 3.3.1.2. ImageJ software was used to calculate the area of reinforcement, and that of penetration. By the data of reinforcement area and penetration area, total area was calculated. Hence, Percentage Dilution could be calculated easily. Before taking macro images, the mounted samples, need to be dry and wet polished. Otherwise, the penetration boundary could not be seen clearly.

Fig. 3.3.1.1 Stereo Zoom Microscope, with mounted monolayer sample

Fig. 3.3.1.2 Stereo Zoom Microscope with macro image shown on monitor

3.3.2 Tensile Testing

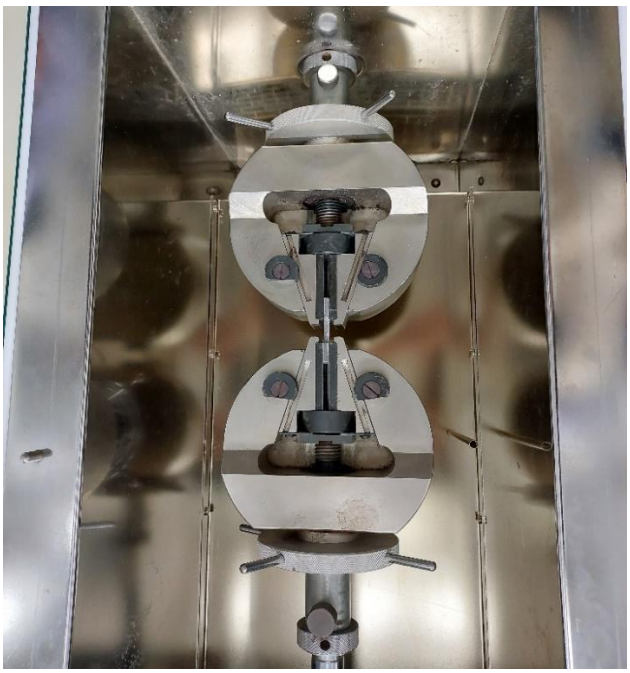

Fig. 3.3.2.1 Dog shaped sample clamped for Tensile Test on Universal Testing Machine (UTM)

To determine the tensile strength of the two samples of top and bottom zone, tensile testing is carried on a Universal Testing Machine (UTM) as shown in Fig. 3.3.2.1, Fig. 3.3.2.2 and Fig. 3.3.2.3. The specimen for the same is prepared according to the ASTM-E8 standard is used for preparing the samples for testing, and are cut by wire electrical discharge machining (EDM), in the form of the shape of a dog bone. At ambient temperature, the prepared specimens undergo tensile testing at an ongoing cross-head velocity of 1 mm/min.

Fig. 3.3.2.2 Dog shaped sample after fracture on UTM

Fig. 3.3.2.3 Readings obtained on UTM, during Testing

3.3.3 Microhardness Testing

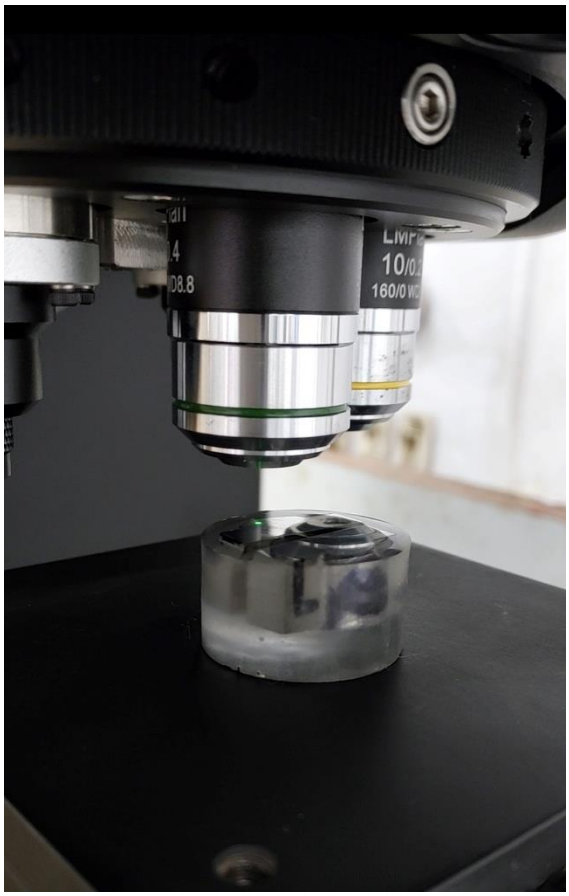

Fig. 3.3.3.1 Positioning the place of indent, shown by green dot

It measures material hardness or penetration resistance. When testing tiny or thin samples or small sections of made samples on Duramin 40 struers hardness tester, as shown in Fig. 3.3.3.1, During the Vickers microhardness test, an indenter of diamond shape is inserted into the outermost layer of the material using a penetrator and a mild burden (300 grams).

When a load is applied to the material, it penetrates the depression, resulting in an irreversible deformation of the material's surface in the form of the indenter. For a square-shaped diamond indenter, the test is conducted under controlled conditions through tracking force for an allotted period (dwell period of 15 seconds). The diagonal arising from an indentation on the material's surface is measured and the Vickers hardness value is calculated using a formula. Fig 3.3.3.2 shows making indent on mounted monolayer cross section by Duramin 40 struers hardness tester, and is displayed on 3.3.3.3.

Fig. 3.3.3.2 Making indent on mounted monolayer cross section by Duramin 40 struers hardness tester

Fig. 3.3.3.3 Monitor showing indent

3.3.4 Optical Microscopy

As depicted in Figure optical microscopy is performed using an Olympus compact GX41 metallurgical inverted microscope, as shown in Fig. 3.3.4.1. The GX41 inverted metallographic microscope is ideal for the rapid and precise analysis of materials and for checking if mechanical properties meet product specifications. Its lightweight and compact body makes portability easier. Portability, Optimal Eyepoint Adjustment, and Outstanding Picture Clarity and Definition with Polarised Lighting are its few distinguishing features.

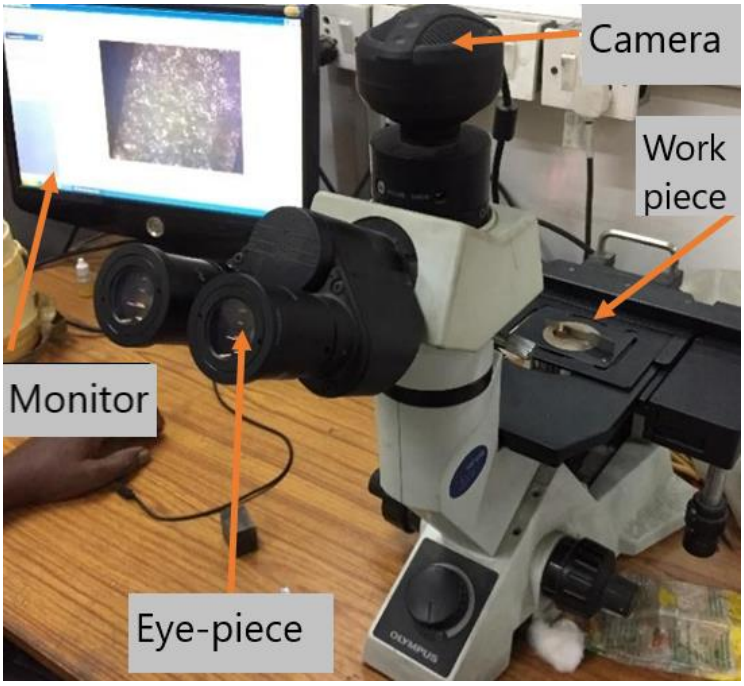

Fig. 3.3.4.1 Monitor showing microstructure

3.4 PROCEDURE

- DOE is made to set input parameters values of current and travel speed.
- RSM is applied to find the optimum process parameters of current and travel speed.
- The heat input, percentage dilution, and microhardness of the monolayers are studied with varying current and travel speeds.
- Based on this optimized parameter by RSM-ANOVA, the first layer of the wall is laid.
- It was learnt from literature review that bidirectional strategy with natural cooling gives sufficient results, and is so followed.
- To prevent the issue of wall collapse due to various reasons, current and travel speed are set in a manner to reduce the heat input as the number of layer increase.
- Current (A), Voltage (V), Wire Feed Speed (m/min), Travel Speed (TS) (cm/min), Heat Input (HI) (J/mm), and Deposition Rate (Kg/hr) is studied for all 27 layers.
- Tensile test, Hardness test, Pore area measurement and microstructural study are done from different zones of build wall.

3.5 FCCD for DOE

For each of the two input parameters, three levels (-1, 0, 1) have been chosen, yielding 3*3 = 9 different input parameter combinations for full factorial experimental design (DOE) as stated in Table 3.5.1.

For greater precision and accuracy, the face-centered composite design (FCCD) provides the repetition of the central value of the DOE. The full factorial design has five repetitions of the central value. To simplify this, in the current model, the central value is repeated three times, giving 11 experiments.

It is applied to get the best input parameters for maximizing microhardness and specifying a target range on % Dilution. The count of the FCCD-designed test is determined using Equation 1. Here, "C" represents the overall count of tests, "f" represents the count of investigated factors, and "r" represents the count of replicates.

$$C = f^2 + 2f + r \quad (1)$$

A value of 1 for Alpha is desirable because it assures the axial position of the point within the factorial element. As stated in Table 3.5.2, it is known as FCCD offers three different stages for the parameters to be incorporated into the DOE matrix.

Table 3.5.1 DOE

Process Parameters	Units	Symbol	Levels		
			-1	0	1
Current	A	I	150	165	180
Travel Speed	cm/min	TS	30	40	50

Table 3.5.2 FCCD for DOE

S.N.	Current (A)	Travel Speed (cm/min)
1	150	50
2	150	30
3	150	40
4	165	30
5	165	50
6	165	40
7	165	40
8	165	40
9	180	30
10	180	50
11	180	40

3.6 MONOLAYER DEPOSITS

$$\text{PD} = \frac{\text{Penetration Area}}{\text{Penetration Area+Reinforcement Area}} * 100 \quad (2)$$

To make a wall of layers, single-layer deposits were studied. Design of Experiment (DOE) was made via face-centered central composite design (FCCD) on the Design Expert software. In CMT synergic mode, there are three dependent parameters of wire feed rate, current, and voltage. Modifying the setting of a single parameter alters the other two parameters. Therefore, between these three, we can study any one parameter only.

The process parameters of welding speed and, current leave a large impact on the characteristics of the monolayer, microstructural characteristics, and mechanical properties. CMT is characterized by low heat input. CMT has an advantage over other processes which show defects due to undergoing temperatures much above their melting point.

Chen [135] worked on Al-Si alloy via WAAM. They worked on the effects of various heat input values on the construction and functionality of manufactured parts. By analyzing the formation, microstructure, and characteristics of WAAM components, a new conceptualization of thermal input is achieved.

Fig. 3.6.1 Samples mounted for polishing

After making mono-layer deposit beads, parallel cuts were made from the centre of each plate perpendicular to its length. A cross-section of the monolayer is obtained by cutting on wire EDM. It was then mounted as shown in Fig. 3.6.1 and then dry polished using various grades of emery paper namely 320, 400, 600, 800, 1000, 1200, 1500, 2000, and 2500, wet polished, and etching was done with Keller's agent (1 ml of HF,1.5 ml of HCl, 2.5 ml of HNO3, and 95 ml of H_2O for 12 seconds).

Macro image were taken on Trinocular stereo zoom microscope with digital camera and PD calculated by the help of ImageJ software, by Eq. 2. Monolayer deposits were then clicked at different magnifications for their micro image, and their dimensions and regions were determined employing a machine.

The micro-hardness of the monolayer deposit and that at different locations (Base metal and Fusion Zone) was measured using a Duramin 40 struers hardness tester. It includes a micro indenter that indents with 300 mN of force for 15 s with a drift time of 5 s. Heat input is calculated for each mono-layer deposit.

3.7 RSM-ANOVA

RSM [136] is a set of mathematical and statistical methods for constructing models. Employing experimental design, the aim is to optimize the several responses which are impacted by the independent parameters. RSM can solve multiple responses, giving more productive solutions with greater precision than other approaches [137]. RSM is an efficient method for determining the optimal quantities of multiple variables in order to achieve the maximum or minimum responses [138].

To make a wall of layers, initially, single-layer deposits were studied. Trials were conducted to study the effect of parameters. Through literature review and trials, it was found that the parameters of current and TS had the most effect on the morphologies of monolayer deposits [139]. In this study, RSM was utilized to optimize the response of Micro Hardness, and % Dilution by modulating the current and TS.

RSM application necessitates establishing the response parameter, defining runs, developing a model framework, optimizing the parameters, and verifying it. Various steps of RSM are-

- The first step: State the response parameter, such as Micro Hardness, and % Dilution.
- Second step: Input of data and its analysis. After collecting the responses, the provided information must be submitted into a database or spreadsheet for assessment.
- Third Step: Construct the RSM model. After data analysis, RSM can be used to develop a statistical framework that describes the correlation amongst the input parameters (like current and travel speed) and the response variables (like Micro Hardness, and % Dilution). This model can be applied to anticipate the response parameter given any combination of input parameters.
- Fourth Step: Optimise the system. It can optimize the welding process by determining the input variables with the most influence on the outcome variables and altering those in order to attain the intended efficiency.

Fifth Step: To check the developed model by evaluating it against fresh data, guaranteeing it's precision and dependability, and its utility to optimize the process of performance [140-142].

In the RSM, it is impractical to conduct a complete factorial experiment where all possible values for every parameter are examined. Rather, the face-centered central composite design (FCCD) fractional factorial method is adopted. The RSM method was implemented using FCCD as it demands lesser runs [139]. Eleven experiments were performed for monolayer deposition, as designed on the software, and analyzed the model through Analysis of variance (ANOVA).

3.8 MULTI-LAYER DEPOSITS

$$\text{Deposition Rate (Kg/hr)} = \eta * \text{Wire Feed Rate} * 60 * \text{kg per metre of wire} \quad (3)$$

The deposition rate is calculated by Eq. 3, η=0.90 for short circuit mode of transfer. Feed wire of AA4047 weighs about 3.5 grams per metre of wire.

The path planning of infill wire deposition is an extremely crucial and decisive factor in the production of WAAM products. There are two ways of path strategies, unidirectional and bidirectional path planning directions. The metal layer is only deposited along one way using the unidirectional procedure. In the reverse orientation, the torch is raised and arrives at the beginning

point (direction of residence). In the bidirectional process, the metal layer is deposited in the back and forth manner.

Due to less wastage of material and increased product credibility, the bidirectional technique is a successful approach for wall-making [143]. Also, better mechanical properties are achieved by the bidirectional technique [144]. Thus, in this work, the wall was constructed using a bidirectional layer deposition strategy, in which each successive layer is deposited in the opposing direction of the preceding layer. Moreover, the Bidirectional torch movement with reduced heat input decreases the humping defect.

The humping defect is the uneven deposition of filler wire. It reduces the positional capability, especially when layers have to be deposited over one another, like in wall fabrication. This defect mainly occurs due to high travel speed [145,146].

Koli et. al. has studied the humping defect on varying current and torch trajectory motion. The humping defect has a significant impact on the elongation and tensile strength. The greater the humping defect, the softer the material becomes, giving reduced hardness levels. Bidirectional motion with reduced heat accumulation reduces humping defect [147].

Chen et. al. [132] made wall fabrication via different methods- by making multiple layers at a constant current without cooling, at a constant current with inter-layer cooling time for 3 mins, by decreasing current by 2 A for each depositing layer without extra interlayer cooling, and by decreasing current by 3 A for first six layers, decreasing current by 2 A for next six layers, and decreasing current by 1 A for next six layers without extra interlayer cooling, to make an 18-layer wall. The study reflected the last method to be the best in terms of uniform width of layers, deposition rate, fabrication time, quality, and morphology of the deposited layers.

Teixeira et. al. [133] increased the travel speed when increasing the deposition layers. They studied various external cooling methods of near immersion active cooling (NIAC). They also studied the interlayer temperature (IT) variations. Regardless of the cooling method (natural cooling (NC) or NIAC)), a more polished look (waviness) is achieved with a greater IT and TS combination when the effective wall width remains the same.

Choosing any of the cooling methods has no effect on the thickness of the wall (average or external) or the height of the layer. Nonetheless, they are influenced by the arrangement of IT as well as TS (the more the IT-TS combination, the narrower and smaller the breadth and height, correspondingly).

Although there was variability in arc energy (in proportion to TS) and IT, no significant microstructural differences were found as an effect of IT in combination with TS when either NC or NIAC was employed. However, tempering was noticed in the layers deposited under NC at temperatures between 300 and 500 degrees Celsius [148]. The average width of the wall reduces from

1.22 to 1.06 mm as the TS increases from 30 cm/min to 42 cm/min, indicating a drop in the melt pool area. Limiting the width of the melt pool boundary provides an additional advantage for UTS, as the huge amount of Silicon particles in the melt pool boundaries happen to degrade readily, thereby diminishing the strength of the alloys [149,150].

Hence, by literature review, it is more viable to decrease current on increasing the number of layer depositions, until threshold current is reached. The threshold current for a particular material is the minimum current required for the proper fusing of its two layers when undergoing WAAM. For the factor of safety, the current is not decreased beyond 110 A, as the threshold current for AA 4047 is 103 A.

On reaching near the threshold current, the current cannot be decreased further. Hence, travel speed is increased to justify the above-mentioned cause. Increasing travel speed can reduce porosity, due to lowered heat accumulation. The diameter of the pores reduces when cooling time and TS are increased.

Cooling time increase can increase the duration of the process, therefore decreasing process efficiency. Hence, it is better to lower the current and increase the TS for overall improvement in wall characteristics. The process parameter for making a wall is selected by the optimized result of RSM. The optimized level of current and welding speeds for monolayer by RSM are 150.211 A and 47.914 cm/min.

Also, in research by Novelino et. al. [143], the horizontal TS finalized after analyzing multiple walls is 8 mm/sec or 48 cm/min. Thus, the first layer of the wall is laid at 150 A and TS of 48 cm/min. After depositing the first layer on AA 6082 substrate, multiple layers are laid. Studies have shown the effect of inter-layer cooling time on the temperature of the deposited layer, affecting the width, and height of each layer [151,152].

According to the literature review, TS can be increased upto 95 cm/min, and researchers have concluded that increasing the travel speed, reduces the pore diameter. Thus, it is beneficial to increase travel speed, and there lies no problem to increase the TS up to 70 cm/min.

There is an overall impact of variation of current and TS for a constant rate of shielding gas on then the operational characteristics of surface finish, fabrication time, and heat input; geometrical characteristics of wall width, and height; and metallurgical characteristics of % dilution, microhardness, and microstructure of multilayer deposits. Heat input, microhardness, strength, and microstructure of the wall are studied in this paper.

A 27-layer thin wall is made by the CMT WAAM process with 45 seconds of inter-layer pause time for natural cooling. To control the width and deposition energy, the current is reduced in Zone A and

Zone B, keeping the travel speed constant. Once the threshold current is reached, the current is kept constant and, travel speed is increased in Zone C, and Zone D.

CHAPTER 4 RESULTS AND DISCUSSION

4.1 MONOLAYER DEPOSITS

4.1.1 Characteristics

To get the optimum heat input for CMT WAAM of AA 4047, several layers can be selected - the third monolayer, made with 150 A current, 40 cm/min TS, 282.6 J/mm of heat input, the fifth monolayer made with 165 A current, 50 cm/min TS, 258.192 J/mm of heat input, and tenth monolayer made with 180 A current, 50 cm/min TS, 292.032 J/mm of heat input, as shown in Table 4.1.1.1. Table 4.1.1.2 shows measured area of deposition.

Table 4.1.1.1 Characteristics of deposited monolayer

Bead	Current (A)	Travel Speed (cm/min)	Reinforcement height (mm)	Width of monolayer (mm)	Depth of Penetration (mm)	Voltage (V)	Heat Input (J/mm)
1	150	50	2.76	7.16	1.31	15.7	226.08
2	150	30	3.26	9.93	2.57	15.7	376.8
3	150	40	2.88	8.74	2.26	15.7	282.6
4	165	30	3.08	11.6	3.46	16.3	430.32
5	165	50	3.05	9.5	2.83	16.3	258.192
6	165	40	2.9	9.8	3.38	16.3	322.74
7	165	40	3.18	9.82	2.61	16.3	322.74
8	165	40	3.05	10.66	3.19	16.3	322.74
9	180	30	3.21	12.64	5.05	16.9	486.72
10	180	50	3.68	11.02	3.77	16.9	292.032
11	180	40	3.2	10.96	4.95	16.9	365.04

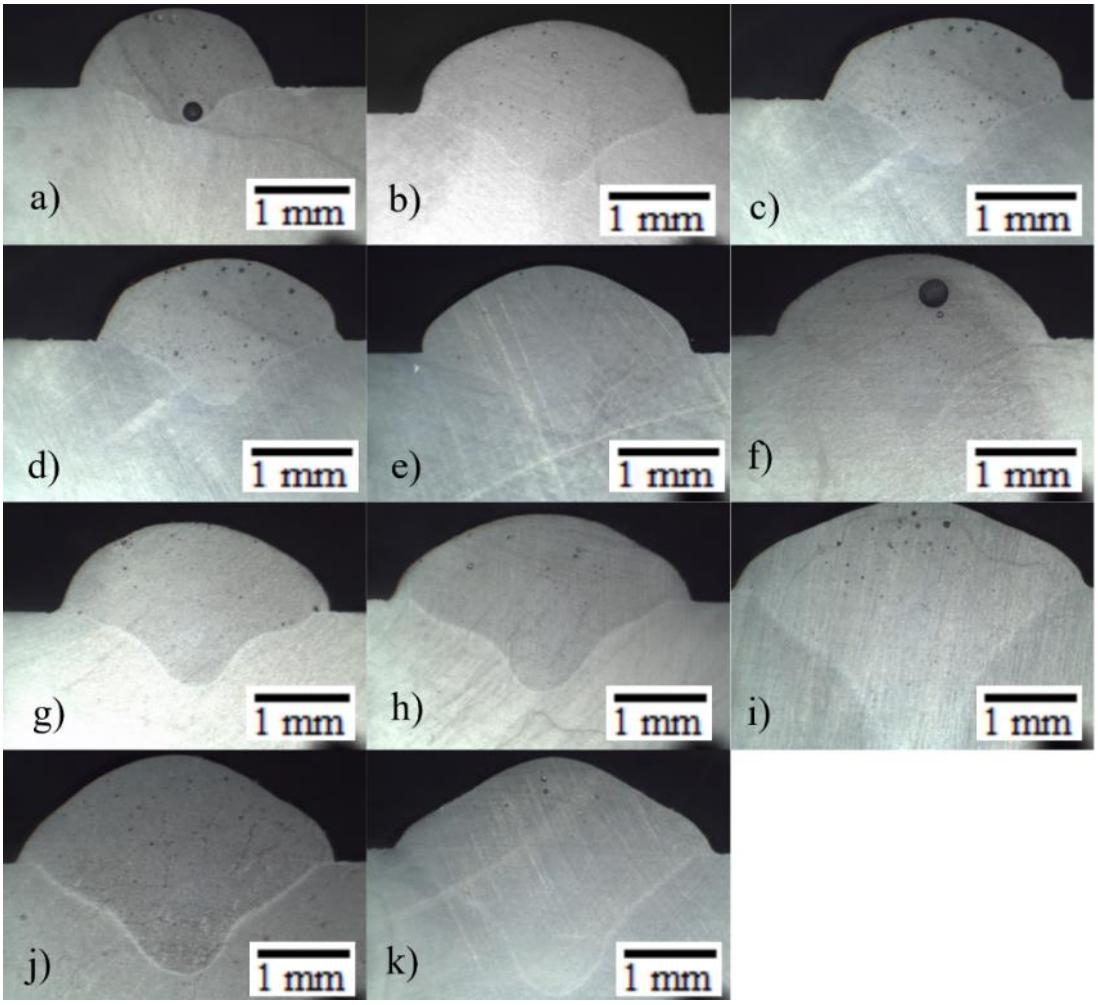

Fig. 4.1.1.1 Macroscopic images of Monolayer (a-k), as per DOE

Table 4.1.1.2 Measured Area of deposition

	Current (A)	Travel Speed (cm/min)	Penetration Area (mm^2)	Reinforcement Area (mm^2)	Total Deposited Area (mm^2)	Macro image
1	150	50	7.1247	11.5753	18.7	Fig. 4.1.1.1 a
2	150	30	13.759	21.25107	35.01	Fig. 4.1.1.1 b
3	150	40	10.233	16.34547	26.578	Fig. 4.1.1.1 c
4	165	30	17.533	26.190676	43.724	Fig. 4.1.1.1 d
5	165	50	12.362	20.255778	32.618	Fig. 4.1.1.1 e
6	165	40	12.785	20.081737	32.867	Fig. 4.1.1.1 f
7	165	40	13.461	20.531772	33.993	Fig. 4.1.1.1 g
8	165	40	13.102	20.067245	33.169	Fig. 4.1.1.1 h
9	180	30	25.1	28.19041	53.29	Fig. 4.1.1.1 i
10	180	50	18.42	24.218384	42.638	Fig. 4.1.1.1 j
11	180	40	22.166	26.657358	48.823	Fig. 4.1.1.1 k

4.1.2 Effect of Process Parameters

Fig. 4.1.2.1 shows that with an increase in welding speed (30–50 cm/min) at constant currents (150 A, 165 A, 180 A), the heat input is reduced by 30% (Fig. 4.1.2.1 a), decreasing width (Fig. 4.1.2.1 b), depth of penetration, reinforcement area (Fig. 4.1.2.1 e), deposited area (Fig. 4.1.2.1 f) and % Dilution (Fig. 4.1.2.1 i), and increasing microhardness (Fig. 4.1.2.1 j). The reinforcement height decreases at a constant current of 150 A and 165 A when TS increases from 30 cm/min to 50 cm/min, but for current 180 A, it almost remains constant between 30 cm/min to 50 cm/min, and increases when travel speed is increased to 50 cm/min. It can be seen that % Dilution is directly proportional to Heat Input (Fig. 4.1.2.1 g) whereas Micro Hardness and Heat Input are inversely proportional (Fig. 4.1.2.1 h).

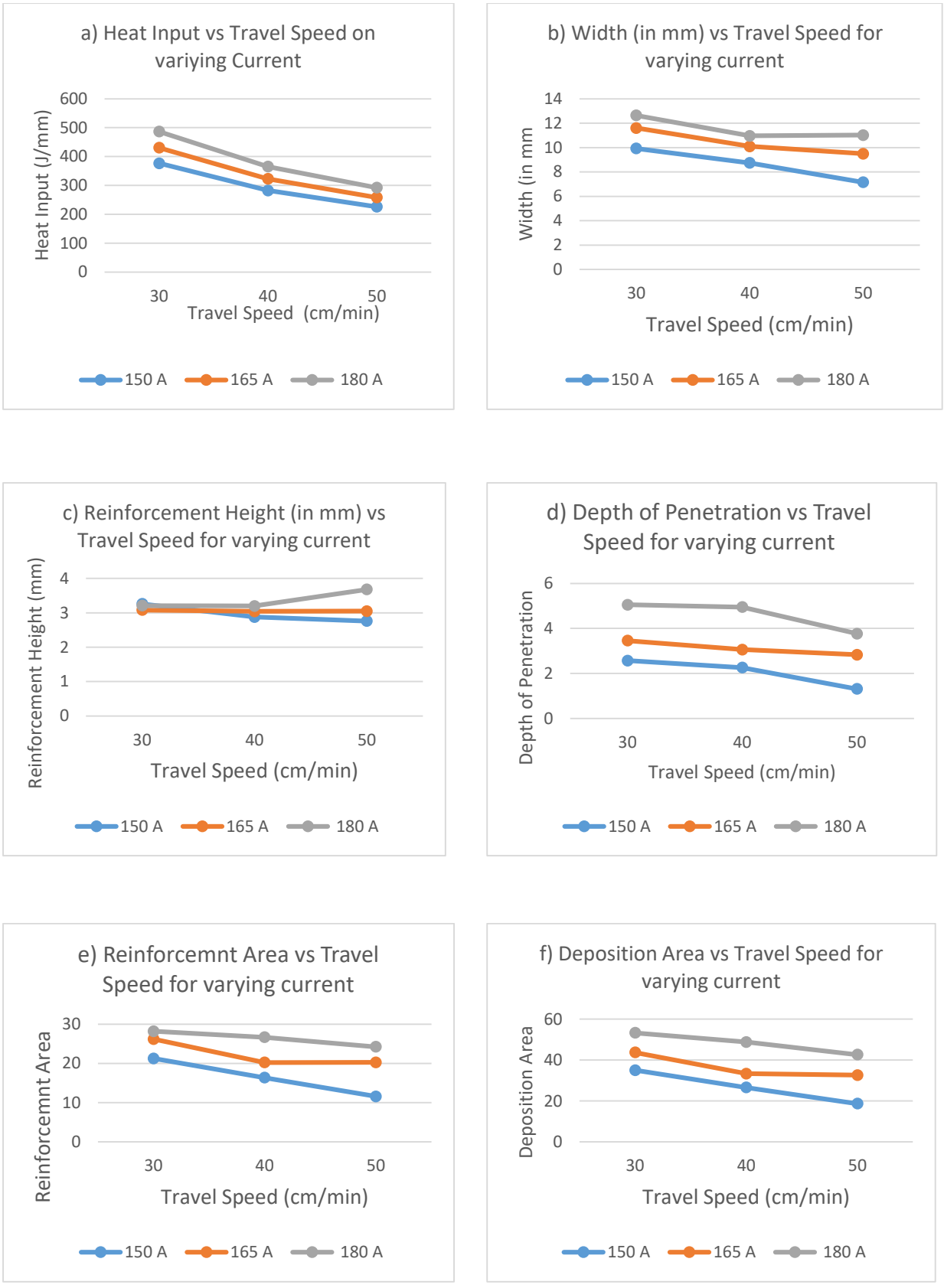

Fig. 4.1.2.1 Characteristic graphs for monolayer (a-f)

4.1.3 Testing of Monolayer samples

Table 4.1.3.1 Hardness and PD of monolayers

SN	Response 1	Response 2
	Hardness (Hv)	PD (%)
1	72.99	0.381
2	69.56	0.393
3	72.43	0.385
4	63.11	0.401
5	69.99	0.379
6	67.89	0.389
7	68.15	0.396
8	67.14	0.395
9	61.23	0.471
10	69.89	0.432
11	66.89	0.454

Fig. 4.1.3.1 shows hardness value parallel to the base from base substrate to monolayer to base substrate. Table 4.1.3.1 shows responses of hardness and PD of monolayers. Highest TS with least current gives maximum hardness. It increases with increase in TS, and decrease in current. PD increases, as current is increased to 180 A, it is not much affected by the TS (Fig. 4.1.3.2). On increasing HI, hardness decreases and PD increases (Fig. 4.1.3.3).

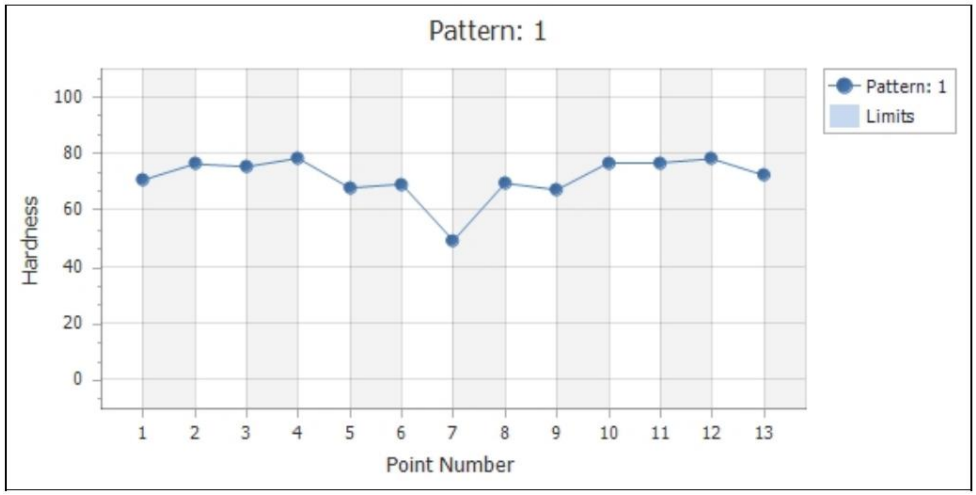

Fig. 4.1.3.1 Hardness parallel to the base from base substrate to monolayer to base substrate

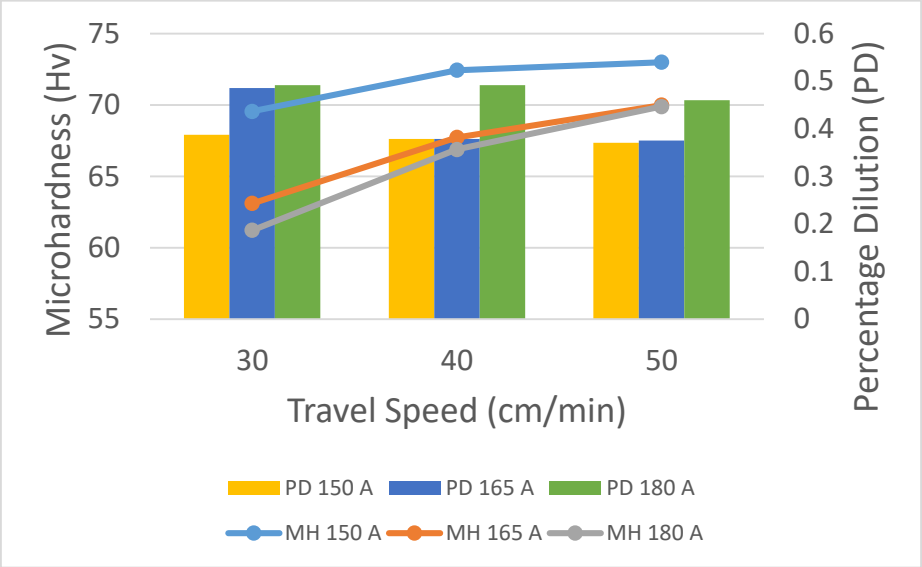

Fig. 4.1.3.2 Micro Hardness, Percentage Dilution (PD) vs Travel Speed for Varying Current

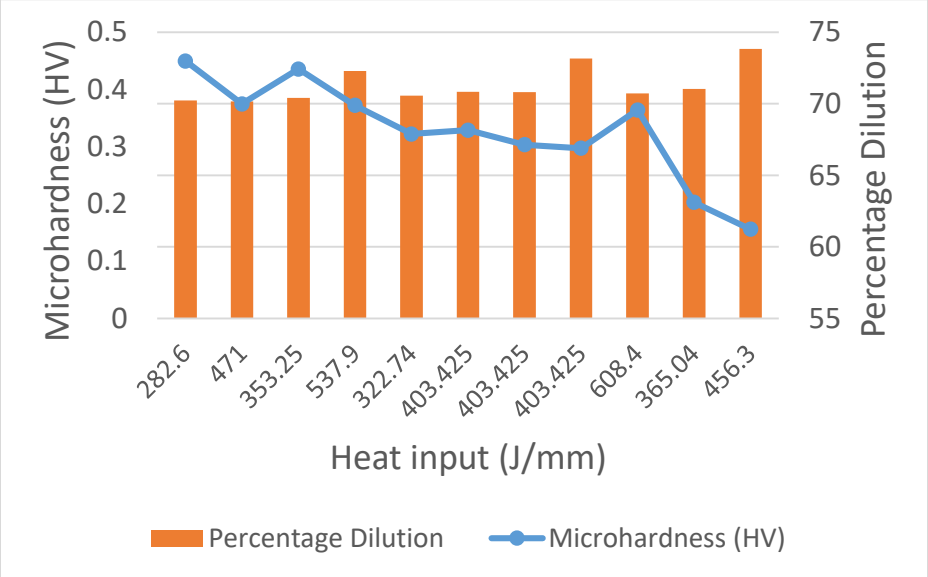

Fig. 4.1.3.3 Micro Hardness, Percentage Dilution (PD) vs Heat Input (HI) for monolayers

At the edges of the melt pool, a coarser microstructure is observed, which is common for Al-Si alloys. Large Si particles are present in bulk in the melt pool boundaries, and columnar grains with nuclei are observable in the melt pool. In the Fig. 4.1.3.4, a transition from equiaxed grains to columnar grains is seen when moving from the center of deposition toward the base metal.

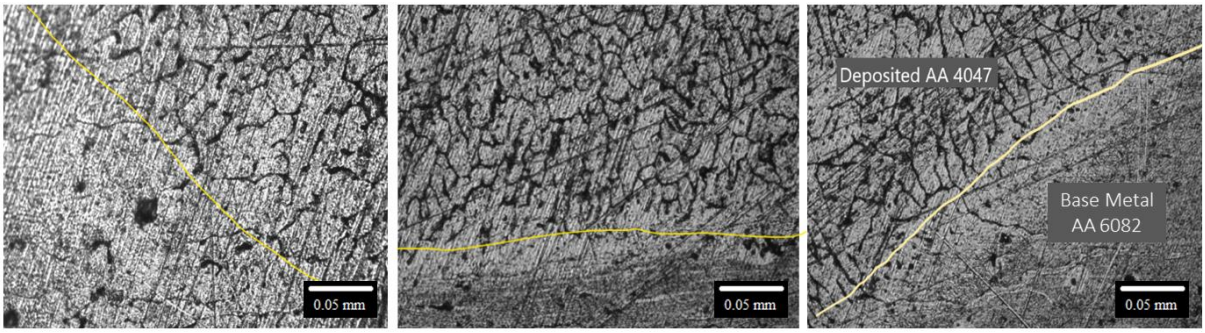

Fig. 4.1.3.4 Showing Boundary region of monolayer deposits

4.2 RSM OPTIMISATION

This paper implements Design Expert software for optimization. Employing the sequential F-test along with the test for lack of fit, and the ANOVA approach, the model's reliability is examined to determine the optimal model. In the current study, RSM is applied to establish the statistical connections among the factors and their responses as shown in Table 4.2.1, in order to determine the optimal monolayer for wall formation.

Table 4.2.1 Factors and their Responses for monolayer deposits

SN	Run	Factor 1 A: Current (A)	Factor 2 B: Travel Speed (cm/min)	Response 1 Micro Hardness (Hv)	Response 2 Percentage Dilution (%)
1	11	150	50	72.99	0.381
2	1	150	30	69.56	0.393
3	8	150	40	72.43	0.385
4	5	165	30	63.11	0.401
5	10	165	50	69.99	0.379
6	9	165	40	67.89	0.389
7	3	165	40	68.15	0.396
8	4	165	40	67.14	0.395
9	2	180	30	61.23	0.471
10	7	180	50	69.89	0.432
11	6	180	40	66.89	0.454

4.2.1 ANOVA for Quadratic Model and Fit Statistics

Table 4.2.1.1 and Table 4.2.1.2 depicts ANOVA for % Dilution and Hardness, respectively. The technique of ANOVA is employed to evaluate the model's significance. The objective of ANOVA is to determine if the CMT WAAM parameters and their interactions have a major influence on the characteristics of the monolayer and to determine whether the model developed is significant or not.

Table 4.2.1.1 ANOVA table of full quadratic for PD

Source	Sum of Squares (SS)	Degree of Freedom (DOF)	Mean Square (MS)	F-value	p-value	
Model	125.3	5	25.06	157.53	< 0.0001	significant
A-Current	48	1	48	301.71	< 0.0001	
B-Travel Speed	59.98	1	59.98	377.01	< 0.0001	
AB	6.84	1	6.84	42.98	0.001	
A^2	9.13	1	9.13	57.41	0.000	
B^2	3.72	1	3.72	23.37	0.004	
Residual	0.7954	5	0.1591			
Lack of Fit	0.2454	3	0.0818	0.2974	0.828	not significant
Pure Error	0.5501	2	0.275			
Cor Total	126.1	10				
				R^2	0.9937	
Std. Dev.	0.3989			Adjusted R^2	0.9874	
Mean	68.12			Predicted R^2	0.9714	
C.V. %	0.5856			Adeq Precision	40.67	

Table 4.2.1.2 ANOVA table of full quadratic model for hardness

Source	Sum of Squares (SS)	Degree of Freedom (DOF)	Mean Square (MS)	F-value	p-value	
Model	125.3	5	25.06	157.53	< 0.0001	significant
A-Current	48	1	48	301.71	< 0.0001	
B-Travel Speed	59.98	1	59.98	377.01	< 0.0001	
AB	6.84	1	6.84	42.98	0.0012	
A^2	9.13	1	9.13	57.41	0.0006	
B^2	3.72	1	3.72	23.37	0.0047	
Residual	0.7954	5	0.1591			
Lack of Fit	0.2454	3	0.0818	0.2974	0.8287	not significant
Pure Error	0.5501	2	0.275			
Cor Total	126.1	10				
				R^2	0.9953	
Std. Dev.	0.003			Adjusted R^2	0.9906	
Mean	0.4069			Predicted R^2	0.9785	
C.V. %	0.7414			Adeq Precision	41.235	

Table 4.2.1.1 and 4.2.1.2 shows the ANOVA results for the response. It displays SS, DOF, and mean square (MS) is the ratio of SS to DOF, F value, and P value. The F-value is the proportion of factor variance to within-factor variance.

The P value represents the chance and is lower than 0.05 for the model terms to be significant. For % Dilution, A, B, AB, A^2 are the model terms with significance whereas for Micro Hardness, A, B, AB, A^2, B^2 are the model terms with significance.

Both the tables for ANOVA display the complete quadratic model for % Dilution, and Hardness, as each of the model terms, which include relationships among input parameters (AB), are statistically significant. It is good to have a non-significant lack of fit, both cases have a non-significant lack of fit.

The variation in adjusted R2 and predicted R2 is lower than 0.2 for all response parameters. The utmost number of points that lie within the line of regression is determined by the similarity of the predicted and revised R2 values.

The primary distinction between the predicted R2 and revised R2 is that predicted R2 implies that the change of the dependent variable can be analyzed by each individual variable. A sufficient level of precision corresponds to a signal-to-noise ratio (S/N) that is greater than 4. According to the result of % Dilution and Hardness in the ANOVA, it is higher than that of 4, indicating adequate signal.

4.2.2 Model Equations

The following are the absolute statistical equations derived from actual response factors. By juxtaposing the factor coefficients, these equations are utilized to study the respective importance of the factors.

$$\%\ \text{Dilution} = +3.11651 - 0.036758 * \text{Current} + 0.007577 * \text{Travel Speed} - 0.000045\ \text{Current} * \text{Travel Speed} + 0.000124 * \text{Current}^2 - 0.000017 * \text{Travel Speed}^2 \quad (4)$$

$$\text{Micro Hardness} = +354.09526 - 3.32196 * \text{Current} - 0.153031 * \text{Travel Speed} + 0.008717 * \text{Current} * \text{Travel Speed} + 0.008439 * \text{Current}^2 - 0.012113 * \text{Travel Speed} \quad (5)$$

4.2.3 Graphs for RSM-ANOVA

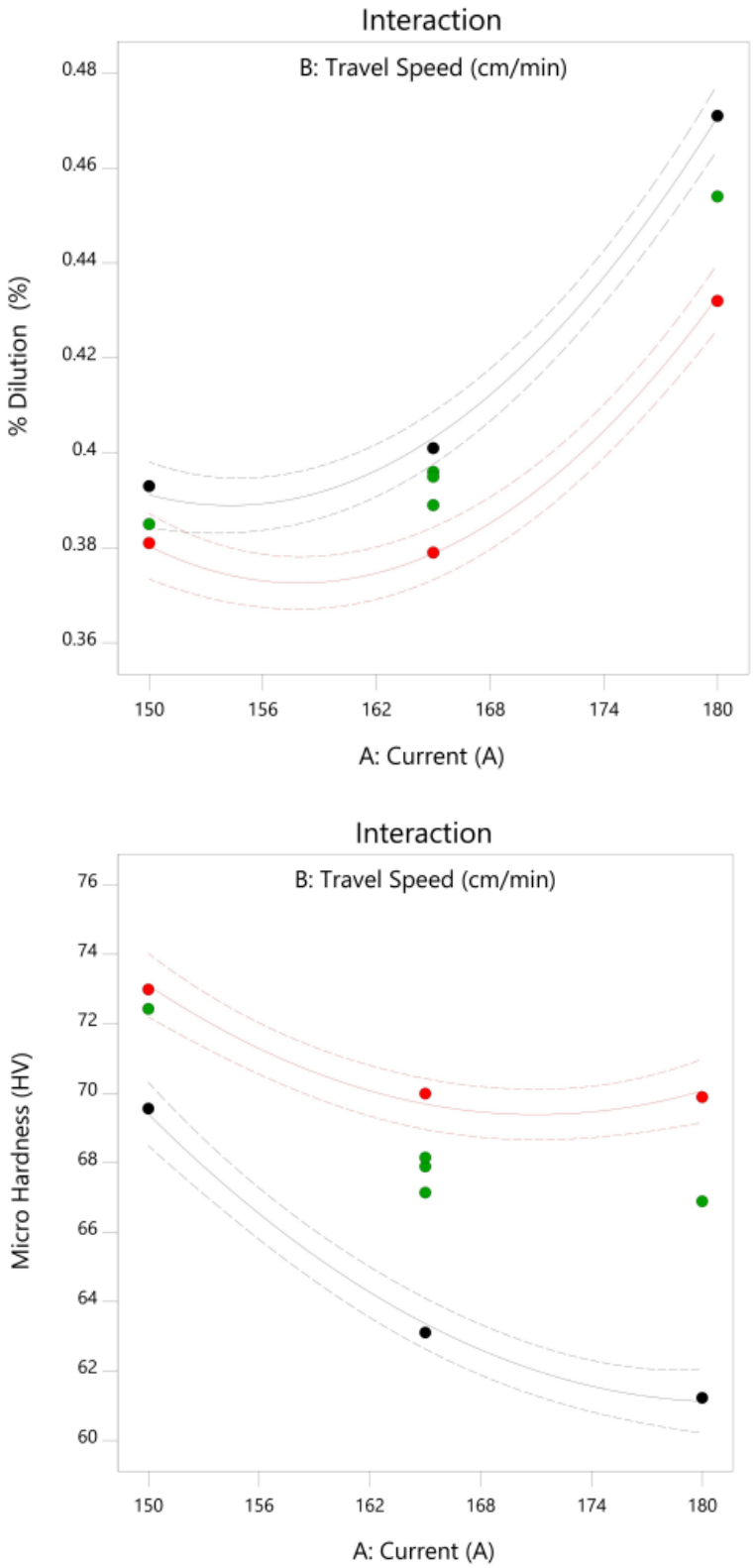

Fig 4.2.3.1. Interaction curve of input and output parameters for % Dilution and Micro Hardness

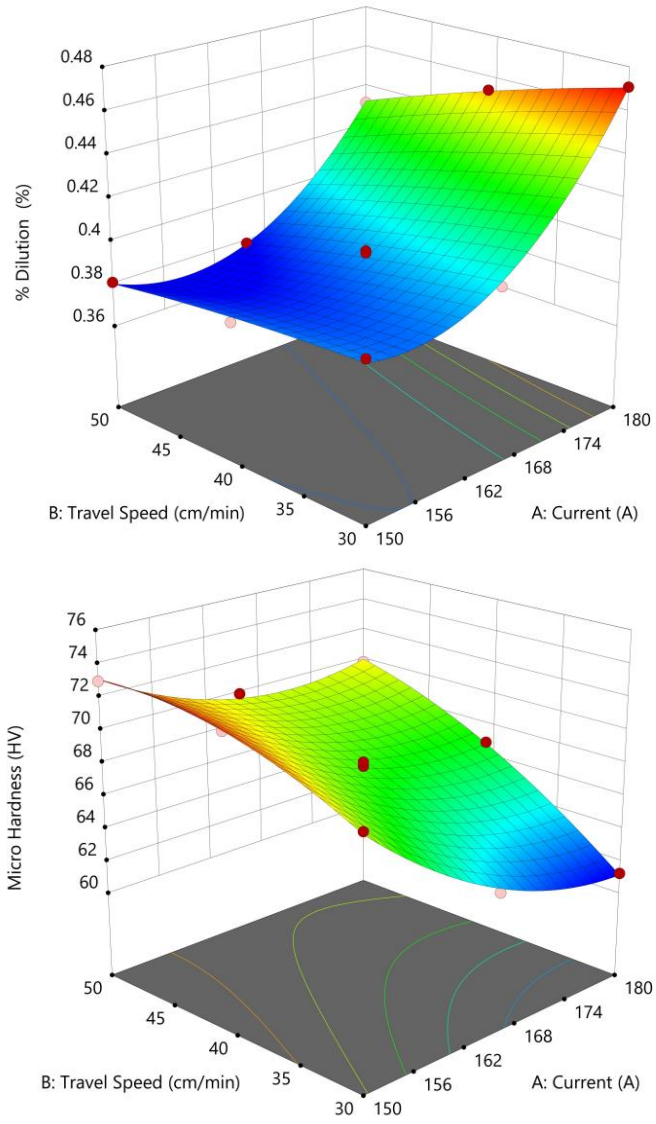

Fig. 4.2.3.2 3-D surface plot of input-output parameter interaction for CMT-WAAM.

Fig 4.2.3.1 shows interaction curve of input and output parameters for % Dilution and Micro Hardness. Figure 4.2.3.2 depicts the 3D surface plot of the interaction of input-output parameters for CMT-WAAM. The Fig. 4.2.3.3 depicts the predicted versus actual response, that approximately fits, showcasing the applicability of the quadratic regression equations, and concluding the significance of the model. A higher value of % dilution results in a lower reinforcement height and deeper penetration. In such cases, dilution should be between 35 and 45 percent, as discussed by numerous scientists and researchers.

CMT accomplishes satisfactory dilution by conserving nearly fifty percent of the energy required. Too much dilution results in the formation of cavities (burn-through), while too little dilution leads to a lack of bonding. CMT can yield lower dilution (less than 5%) for cladding purposes.

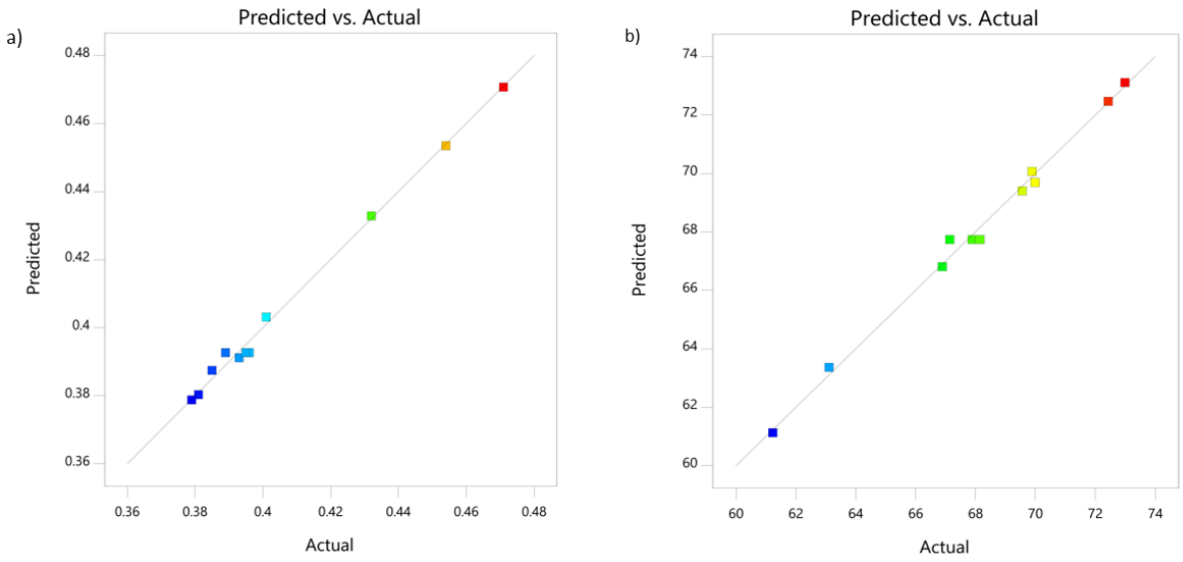

Fig. 4.2.3.3 Predicted vs Actual values for CMT-WAAM for PD (a), and hardness (b)

4.2.4 Optimal Parameters

Optimization of WAAM parameters on design expert software identifies a set of levels of factors or ranges that simultaneously satisfy essential optimization criteria on all response as well as process parameters. The RSM's optimization of the desirability function is utilized optimization. Using the process of optimization, a target was established to maximize micro hardness while keeping dilution in range.

In CMT joining high dilution is required to get good strength of the joint. Such high dilution is not required for the base monolayer, as further layers have to be built on the monolayer for making a thin wall, and the base has to be kept strong enough to retain the wall load. High dilution can also create a high HAZ, altering base metal properties, and is thus kept in range. The Table 4.2.4.1 shows the criteria of optimal parameters, and Table 4.2.4.2 shows optimized results for optimal parameters.

Table 4.2.4.1 Criteria for optimal parameters

Name	Goal	Lower Limit	Upper Limit	Lower Weight	Upper Weight	Importance
A: Current	is in range	150	180	1	1	3
B: Travel Speed	is in range	30	50	1	1	3
Micro Hardness	maximize	61.23	72.99	1	1	3
% Dilution	is in range	0.38	0.43	1	1	3

Table 4.2.4.2 Optimized results for optimal parameters

Number	Current	Travel Speed	Micro Hardness	% Dilution	Desirability	
	A	cm/min	Hv	%		
1	150.211	47.914	73.098	0.382	1.000	Selected
2	150.158	44.945	73.025	0.384	1.000	
3	150.009	48.249	73.170	0.382	1.000	
4	150.028	49.002	73.145	0.381	1.000	
5	150.000	50.000	73.110	0.380	1.000	
6	150.188	48.938	73.089	0.381	1.000	
7	150.048	44.867	73.064	0.384	1.000	
8	150.333	47.784	73.053	0.382	1.000	
9	150.219	47.560	73.095	0.382	1.000	
10	150.417	47.272	73.019	0.382	1.000	
11	150.193	47.462	73.104	0.382	1.000	
12	150.226	46.557	73.076	0.383	1.000	
13	150.294	45.347	72.997	0.384	1.000	
14	150.287	49.402	73.038	0.380	1.000	
15	150.311	46.810	73.050	0.382	1.000	
16	150.248	46.716	73.072	0.383	1.000	

Table 4.2.3.2 depicts the optimal parameters, in decreasing order of desirability value. RSM method generated 54 solutions out of which 45 have desirability 1. The optimum level of current and TS are 150.211 A and 47.914 cm/min, respectively with 100 % desirability.

The optimum parameters produce results of in-range dilution (38.2 %) and maximal microhardness (73.098 Hv), resulting in an aesthetically pleasing monolayer for effective wall construction. The confirmation test is a supplementary run conducted at the optimal parameter combination. The mean of the confirmation test response is contrasted with the model's prediction interval.

If the mean data from the validation trial falls within the prediction interval of the validation node, the model is validated. To confirm the model, three validation tests were performed. Using the software's point prediction ability, the outcomes were estimated with a confidence level of 95%. Model equations were used to compute the predicted values of dilution and microhardness.

4.3 MULTILAYER WALL FABRICATION

Multilayer wall is made on the optimized parameter. Thus, the first layer of the wall is laid at 150 A and TS of 48 cm/min. A 27-layer thin wall is made by the CMT WAAM process with 45 seconds of inter-layer pause time for natural cooling. To maintain the uniform width of the wall and to overcome the molten pool overflow, due to reheating, arc energy is made to decrease on increasing the number of deposition layers by either decreasing current or increasing the TS.

For overall improvement in characteristics of build AA 4047 wall, initially current is decreased (up to the threshold current) and then TS is increased. The threshold current is the minimum current for the proper fusing. Once the threshold current is reached, the current is kept constant and, travel speed is increased in Zone C, and Zone D. For the factor of safety, the current is not decreased beyond 110 A. The wall is built in 4 zones, as shown in Table 4.3.1.

The current is reduced in Zone A and Zone B to 130 A and 114 A respectively, keeping the TS constant. Then, the current is kept constant at 112 A, and 110 A and, TS is increased to 54 cm/min and 61 cm/min respectively in Zone C, and Zone D. Thus, it is harmless to increase TS up to 61 cm/min.

Table 4.3.1 Zone wise, process parameters for making multilayer wall

Overall Layer No.	ZONES	Zone Wise Layer No.	Current (A)	Voltage (V)	Wire Feed Speed (m/min)	Travel Speed (TS)	Heat Input (HI)	Deposition Rate (Kg/hr)	Remarks
1	ZONE	1	150	15.7	9.1	48	235.5	1.4742	4 times
2	A	2	145	15.4	8.9	48	223.3	1.4418	5 A drop
3		3	140	15.2	8.7	48	212.8	1.4094	in
4		4	135	15	8.5	48	202.5	1.377	current
5		5	130	14.8	8.3	48	192.4	1.3446	
6	ZONE	1	128	14.8	8.2	48	189.44	1.3284	9 times
7	B	2	126	14.7	8.1	48	185.22	1.3122	2 A drop
8		3	124	14.6	8	48	181.04	1.296	in
9		4	122	14.5	7.9	48	176.9	1.2798	current
10		5	120	14.5	7.8	48	174	1.2636	
11		6	118	14.4	7.7	48	169.92	1.2474	
12		7	116	14.4	7.7	48	167.04	1.2474	
13		8	114	14.3	7.6	48	163.02	1.2312	
14	ZONE	1	112	14.2	7.5	48	159.04	1.215	
15	C	2	112	14.2	7.5	49	155.7943	1.215	6 times,
16		3	112	14.2	7.5	50	152.6784	1.215	1
17		4	112	14.2	7.5	51	149.6847	1.215	cm/min
18		5	112	14.2	7.5	52	146.8062	1.215	hike in
19		6	112	14.2	7.5	53	144.0362	1.215	TS
20		7	112	14.2	7.5	54	141.3689	1.215	
21	ZONE	1	110	14.1	7.4	55	135.36	1.1988	6 times,
22	D	2	110	14.1	7.4	56	132.9429	1.1988	1
23		3	110	14.1	7.4	57	130.6105	1.1988	cm/min
24		4	110	14.1	7.4	58	128.3586	1.1988	hike in
25		5	110	14.1	7.4	59	126.1831	1.1988	TS
26		6	110	14.1	7.4	60	124.08	1.1988	
27		7	110	14.1	7.4	61	122.0459	1.1988	

Fig. 4.3.1 shows the build wall. The measured wall height (Fig.4.3.2 a), wall length (Fig. .4.3.2 b) was 10 cm, 5 cm and the wall thickness reduced from 8 mm to 7.3 mm after flattening. The side of the substrate material is cut out and the wall surface is made flat from at least one side-by-end milling.

Electric Discharge Machine is used for cutting out test samples. Two samples are cut for tensile testing, three samples are cut for hardness, and three more samples are cut for the micro image of the microstructure on the wall, from different zones, as seen in Fig. .4.3.2 c.

Fig. 4.3.1 CMT-WAAM made AA4047 wall

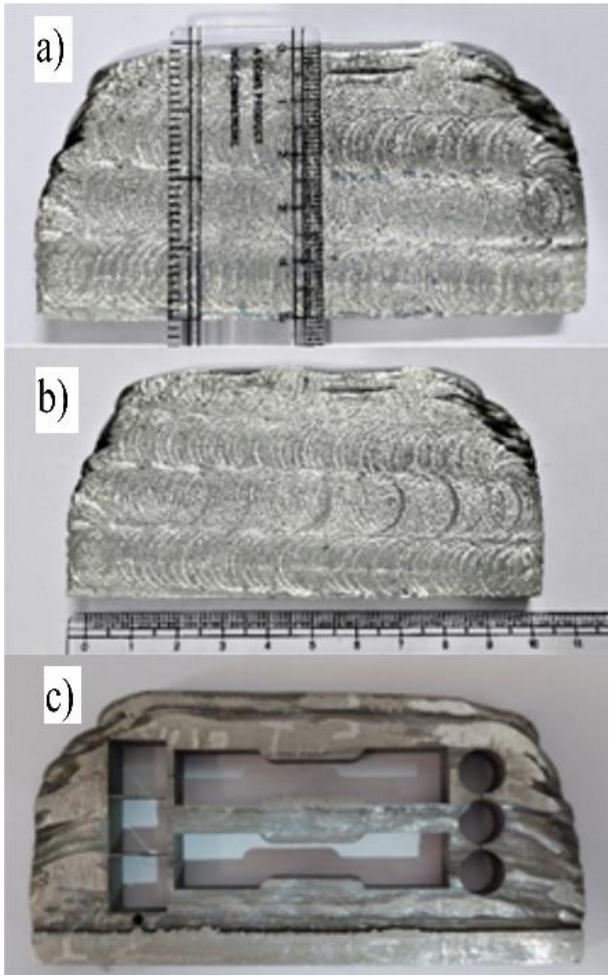

Fig. 4.3.2 Height (a) and Length (b) of the built wall, Samples cut from wall (c) for various tests

4.4 TEST RESULTS AND DISCUSSION FOR WALL SAMPLES

For tensile testing, wall is divided into 2 zones, whereas for microhardness, and pore area measurement, wall is divided into three zones. The Table 4.4.1 depicts the elastic modulus, yield strain, yield strength (YS), percentage elongation, UTS, microhardness, and pore area of the cut samples from bottom to the top.

Table 4.4.1 Test results on wall samples

S.No.	Elastic Modulus	Yield Strain	Yield Strength	Ultimate Tensile Strength	Percentage Elongation	Micro Hardness	Pore Area
Symbol	E	ϵ	YS	UTS	EL	MH	PA
Unit	MPa		MPa	MPa	%	Hv	mm^2
1 (Bottom Zone)	1142.9	0.71	67	144.3089	31.7	48.405 (Fig. 4.4.1 a)	0.1032
2 (Middle Zone)	-	-	-	-	-	48.56 (Fig. 4.4.1 b)	0.0635
3 (Top Zone)	922.26	0.78	68	148.814	30.9	52.73 (Fig. 4.4.1 c)	0.0410

The average microhardness was 49.90 HV, as depicted in Fig. 4.4.1 (a-c), measured on Duramin 40 struers hardness tester. This is due to the difference in IT among added layers and the existence of coarse particles and tiny pores between layers, which results in a decreased microhardness.

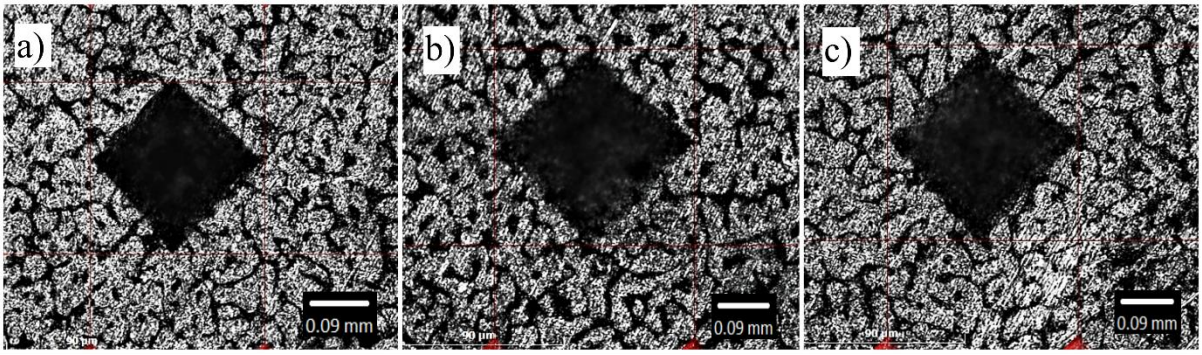

Fig. 4.4.1 Indent by Microhardness test on bottom zone (a), middle zone (b), top zone (c)

If the parameters were kept constant, the lower zone had higher hardness than the top zones, due to heat accumulation by reheating in the top zone. The presence of HAZ in the sampling position can lead to variations in microhardness. HI is decreased as the number of build layers is increased, by decreasing current and increasing TS. Thus, it is swifter to cool the top layers with lower HI, giving them higher hardness.

Fig. 4.4.2 shows tensile testing machine (Fig. 4.4.2 a), samples before (Fig. 4.4.2 b) and after fracture (Fig. 4.4.2 c). The stress strain curve for samples 1 and 2 (bottom and top zone, respectively) is shown in Fig. 4.4.3 a, and the equation of their trend line is shown in Table 4.4.2. The average UTS of these materials is approximately 146.5615 MPa. UTS/YS are proportional to wall height.

From literature review, it is clear that the mechanical properties are generally isotropic, with only a 3–8 MPa variation in ultimate tensile strength (UTS), and a 2–11 MPa variation in yield strength (YS). Analyzing the strength of specimens collected at various current and TS levels, the UTS of these materials is approximately 146.5615 MPa. UTS/YS follows an upward trend. As TS increases from 48 cm/min to 61 cm/min, UTS increases from 144.31 MPa to 148.814 MPa.

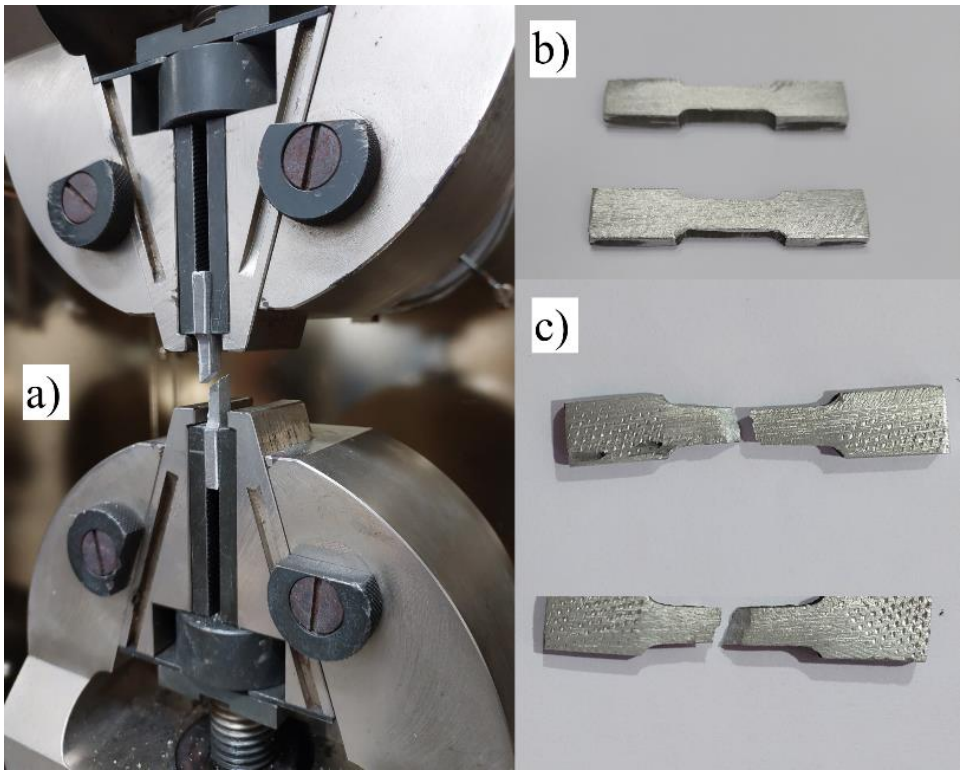

Fig. 4.4.2 Universal Testing machine (a), samples before (b), and after Tensile Test (c)

Table 4.4.2 Equation of stress strain trend line and their R^2

S.No.	Mathematical Equation of Stress Strain Trend Line	R2 of trend line
1	y = -79,60,506.58x6+72,15,471.13x5-24,74,693.82x4+4,01,581.90x3-33,522.98x2+2,101.43x+1.09	0.9688
2	y = -1,19,63,347.48x6+1,02,29,390.86x5-32,79,215.71x4 4,84,198.42x3-34,075.28x2+1,823.37x- 2.08	0.97

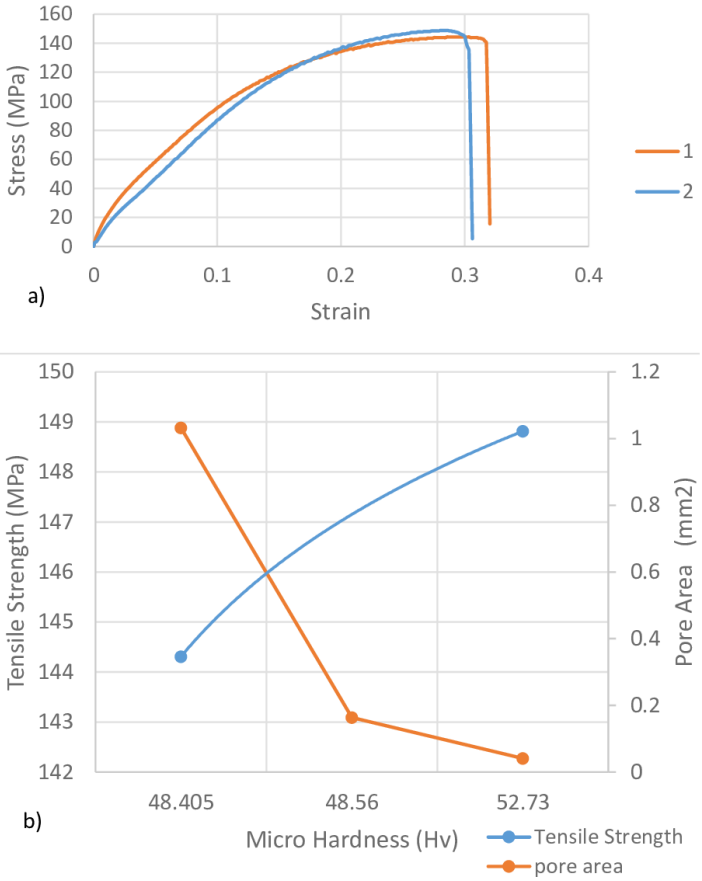

Fig. 4.4.3 Stress Strain diagram for two samples, 1 and 2 (a), and variation of tensile strength, and pore area with microhardness (b)

Also, percentage elongation (PE) in this study is not related to current or TS. On decreasing HI, PE decreased. This trend of PE being directly proportional to HI, is not seen in ER 5356 walls or AA4043 walls. Such unexpected behaviour of AA4047, can own due to its characteristic of lower ductility, or its requirement of repeated annealing for drawing it into wires.

Hence, as the raw AA4047 wire has low PE, so is reflected in the wall samples. Keist et. al. [158] concluded that on increasing hardness, UTS increases. The same trend is observed here, as shown in Fig. 4.4.3.b Sufficient cooling rates in the interlayer regions, lead to the formation of equiaxed

dendrites, single and bi-nuclei formation, along with the fine-grain structure promoting enhanced microstructure, as shown in Fig. 4.4.4 (a-d).

Significant columnar grains in the interlayers got transformed into fine equiaxed grains by modifying the HI. To minimize the diameter of the equiaxed grain and to lower the volume fraction, the TS was increased by decreasing HI levels. At reduced current values, finer grains and uniform microstructure were developed as a result of the quick cooling of the material.

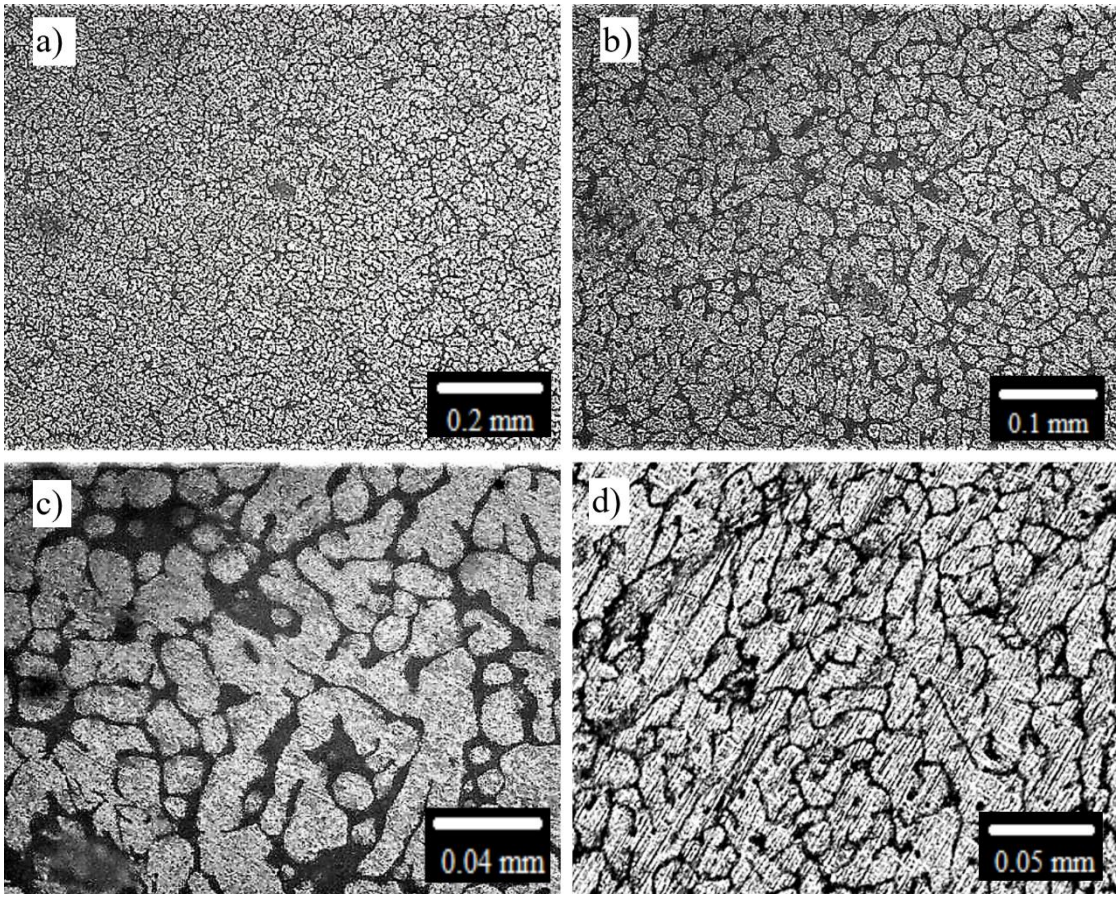

Fig. 4.4.4 Microstructural images (a-c) by Optical Microscope, and showing nuclei formation (d) by Duramin 40 Struers micro image camera

WAAM components have porosity due to turbulent mixing, shielding gas flow rates, and dynamic gas pressure. The shielding gas flow rate affects the number of holes in aluminium components because the convective cooling accelerates melt pool solidification, preventing process-associated gas bubbles from escaping. Cavities are made by gas inclusions that have left from the melt pool. More cavities on the surface means fewer pores in the component [159].

Pores are predominantly close to layer boundaries. Porosity is present more in the first and second layers of deposition. Hence, the current is kept high at the bottom layers, to enable proper penetration

and bonding, reducing the chances of lower strength. The average pore area is 0.0692 mm2. The average porosity percentage reduces as TS increases.

Reduced current, and increased TS, reduces the porosity. Still, in some places large pores were found. The defects can be reduced by using the circling motion planning, instead of the typical hatching trajectory motion of the torch. Circling can increase strength, and reduce the defects, pore size and the porosity area percentage.

Because of an elevated deposition temperature, circling can produce a stronger accumulation with a lesser threat of humping, needing no requirement of process parameter variation [160,161]. Circling motion planning is beyond the scope of this work and can be taken as Future Scope.

CHAPTER 5 CONCLUSIONS

This work had the aim to understand the effect of CMT-WAAM process parameters on the characteristics of the deposited AA 4047. The work comprised 2 deposition groups- monolayer and multilayer deposits. Current and TS, were the most influencing parameters. The RSM method was implemented using FCCD. DOE was designed on the software and analyzed the model through Analysis of variance (ANOVA). The monolayer deposits were analyzed for reinforcement height, layer width, depth of penetration, percentage dilution, microstructure, and microhardness, with respect to varying travel speed, at different current and heat input values. Based on optimized parameters, a 27-layer wall was made and analyzed for heat input, PE, microhardness, strength, porosity, and microstructure. It can be concluded that:

- With an increase in welding speed (30–50 cm/min) at constant currents (150 A, 165 A, 180 A), the heat input is reduced to almost 30% of the initial value, decreasing the width of layer, depth of penetration, reinforcement area, deposited area and Percentage Dilution, and increasing microhardness for the deposited monolayer.
- Hardness is maximum for the highest TS with least current. Microhardness increases with increasing TS, and decreasing current.
- Hardness and HI are inversely proportional to each other, and PD increases slightly on increasing the HI.
- The optimized parameters for current and TS were 150 A and 48 cm/min, respectively, for a constant rate of shielding gas.
- The optimal parameters produced results for the values of in-range dilution (38.2 %) and maximal microhardness (73.098 Hv), resulting in an aesthetically pleasing monolayer.
- There was a need to decrease the current and increase the travel speed, on increasing the number of layer depositions, to manage the heat accumulation in the layers.
- The width of layers was maintained constant, decreasing the heat input, while increasing the height of the wall.
- Average microhardness of 49.90 HV, yield strength of 67.5 MPa, elastic modulus of 1032.58 MPa, PE of 31.3, and UTS of 146.5615 MPa were achieved for the built wall.
- Tensile strength and microhardness increased, as heat input decreased on going upwards in the wall.
- Percentage elongation decreased, as heat input decreased on going upwards in the wall, justifying the raw material property of AA 4047.
- Tensile Strength and Hardness were proportional to each other.

REFERENCES

1. Vipin Gopan, “Innovative potential of additive friction stir deposition among current laser based metal additive manufacturing processes: A review” *CIRP Journal of Manufacturing Science and Technology*, 2021 32, 228-248
2. Gardan J. “Additive manufacturing technologies: state of the art and trends”. In: *Addit. Manuf. Handb*. Prod. Dev. Def. Ind. CRC Press; 2017 p. 149–68. https:// doi.org/10.1201/9781315119106.
3. Technical Committee AMT/8. In: BS EN ISO/ASTM 52900: additive manufacturing - general principles - terminology. Int. Stand.; 2017 p. 1–30.
4. W.E. Frazier, “Metal additive manufacturing: A review”, *J of Mater Eng and Perform*, 23, 2014, pp. 1917-1928, 10.1007/s11665-014-0958-z
5. F. Haftlang, H.S. Kim, “A perspective on precipitation-hardening high-entropy alloys fabricated by additive manufacturing”, *Mater Des*, 211, 2021, Article 110161, 10.1016/j.matdes.2021.110161
6. Jamroz W, Szafraniec J, Kurek M, Jachowicz R. “3D printing in pharmaceutical and medical applications – recent achievements and challenges”. *Pharm Res* 2018; 35:176. https://doi.org/10.1007/s11095-018-2454-x.
7. Blakey-Milner B, Gradl P, Snedden G, Brooks M, Pitot J, Lopez E, Leary M, Berto F, du Plessis A. “Metal additive manufacturing in aerospace: a review”. *Mater Des* 2021, ;209:110008. https://doi.org/10.1016/j.matdes.2021.110008.
8. Gradl PR, Teasley T, Protz C, Katsarelis C, Chen P. “Process development and hotfire testing of additively manufactured NASA HR-1 for liquid rocket engine applications”. In: *American Institute of Aeronautics and Astronautics Inc*, AIAA; 2021. https://doi.org/10.2514/6.2021-3236.
9. Gardner L, Kyvelou P, Herbert G, Buchanan C. “Testing and initial verification of the world’s first metal 3D printed bridge”. *J Constr Steel Res* 2020; 172:106233. https://doi.org/10.1016/j.jcsr.2020.106233.
10. Tofail SAM, Koumoulos EP, Bandyopadhyay A, Bose S, O’Donoghue L, Charitidis C. “Additive manufacturing: scientific and technological challenges, market uptake and opportunities”. *Mater Today* 2018 ;21:22–37. https://doi.org/ 10.1016/j.mattod.2017.07.001.
11. Ziaee M, Crane NB. “Binder jetting: a review of process, materials, and methods”. *Addit Manuf* (2019); 28:781–801. https://doi.org/10.1016/j.addma.2019.05.031.
12. Mirzababaei S, Pasebani S. “A review on binder jet additive manufacturing of 316L stainless steel”. *J Manuf Mater Process* 2019; 3:82. https://doi.org/10.3390/ jmmp3030082.

13. Atapour M, Wang X, Persson M, Odnevall Wallinder I, Hedberg YS. “Corrosion of binder jetting additively manufactured 316L stainless steel of different surface finish”. *J Electrochem Soc* 2020; 167:131503. https://doi.org/10.1149/1945- 7111/abb6cd.
14. Miyanaji H, Zhang S, Yang L. “A new physics-based model for equilibrium saturation determination in binder jetting additive manufacturing process”. *Int J Mach Tool Manuf* 2018; 124:1–11. https://doi.org/10.1016/j. ijmachtools.2017.09.001.
15. Miyanaji H, Yang L. “Equilibrium saturation in binder jetting additive manufacturing processes: theoretical model vs experimental observations”. In: Solid Free. Fabr. 2016 *Proc. 27th Annu. Int. Solid Free. Fabr. Symp. - An Addit. Manuf. Conf*. SFF 2016; 2016. p. 1945–59.
16. Lores A, Azurmendi N, Agote I, Zuza E. “A review on recent developments in binder jetting metal additive manufacturing: materials and process characteristics”. *Powder Metall* 2019; 62:267–96. https://doi.org/10.1080/ 00325899.2019.1669299.
17. Yegyan Kumar A, Bai Y, Eklund A, Williams CB. “The effects of hot isostatic pressing on parts fabricated by binder jetting additive manufacturing”. *Addit Manuf* 2018; 24:115–24. https://doi.org/10.1016/j.addma.2018.09.021.
18. Piscopo G, Iuliano L. “Current research and industrial application of laser powder directed energy deposition”. *Int J Adv Manuf Technol* 2022 :1–25. https://doi.org/ 10.1007/s00170-021-08596-w.
19. Tepylo N, Huang X, Patnaik PC. “Laser-based additive manufacturing technologies for aerospace applications”. *Adv Eng Mater* 2019;21. https://doi.org/10.1002/ adem.201900617.
20. Vafadar A, Guzzomi F, Rassau A, Hayward K. “Advances in metal additive manufacturing: a review of common processes, industrial applications, and current challenges”. *Appl Sci* 2021; 11:1–33. https://doi.org/10.3390/ app11031213.
21. Bouaziz MA, Djouda JM, Kauffmann J, Hild F. “Microscale mechanical characterization of 17-4PH stainless steel fabricated by atomic diffusion additive manufacturing (ADAM)”. In: *Procedia Struct. Integr*. Elsevier B.V.; 2020. p. 1039–46. https://doi.org/10.1016/j.prostr.2020.11.119.
22. Bhaskar Dutta, “Directed Energy Deposition (DED) Technology”, Editor(s): Francisca G. Caballero, *Encyclopedia of Materials: Metals and Alloys*, Elsevier, 2022, Pages 66-84, ISBN 9780128197332, https://doi.org/10.1016/B978-0-12-819726-4.00035-1.
23. Crump SS. United States Patent - US5121329A - apparatus and method for creating three-dimensional objects. 1989.
24. Carroll BE, Palmer TA, Beese AM. “Anisotropic tensile behavior of ti-6Al-4V components fabricated with directed energy deposition additive manufacturing”. *Acta Mater* 2015; 87:309–20. https://doi.org/10.1016/j.actamat.2014.12.054.
25. Gonzalez-Gutierrez J, Cano S, Schuschnigg S, Kukla C, Sapkota J, Holzer C. “Additive manufacturing of metallic and ceramic components by the material extrusion of highly-filled

polymers: a review and future perspectives". *Materials (Basel)* 2018; 11:840. https://doi.org/10.3390/ma11050840.

26. Frazier WE. "Metal additive manufacturing: a review". *J Mater Eng Perform* 2014; 23:1917–28. https://doi.org/10.1007/s11665-014-0958-z.
27. Sames WJ, List FA, Pannala S, Dehoff RR, Babu SS. "The metallurgy and processing science of metal additive manufacturing". *Int Mater Rev* 2016; 61:315–60. https:// doi.org/10.1080/09506608.2015.1116649.
28. Zhang Y, Wu L, Guo X, Kane S, Deng Y, Jung YG, Lee JH, Zhang J. "Additive manufacturing of metallic materials: a review". *J Mater Eng Perform*, 2018 ;27: 1–13. https://doi.org/10.1007/s11665-017-2747-y.
29. A. Zocca, P. Colombo, C.M. Gomes, J. Günster, "Additive manufacturing of ceramics: issues, potentialities, and opportunities", *J. Am. Ceram. Soc*. 98, 2015, 1983–2001.
30. W.E. King, H.D. Barth, V.M. Castillo, G.F. Gallegos, J.W. Gibbs, D.E. Hahn, C. Kamath, A.M. Rubenchik, "Observation of keyhole-mode laser melting in laser powder-bed fusion additive manufacturing", *J. Mater. Process*. 214, 2014, 2915–2925
31. C. Korner, "Additive manufacturing of metallic components by selective electron beam melting-a review*", Int. Mater. Rev*. 61, 2016, 361–377.
32. J.P. Kruth, P. Mercelis, J.V. Vaerenbergh, L. Froyen, M. Rombouts, "Binding mechanisms in selective laser sintering and selective laser melting", *Rapid Prototyp*. J. 11, 2005, 26–36.
33. C.Y. Yap, C.K. ChuaZ, L. Dong, Z.H. Liu, D.Q. Zhang, L.E. Loh, S.L. Sing, "Review of selective laser melting: Materials and applications", *Appl. Phys*. Rev. 2, 2015, 041101.
34. Gibson I, Rosen DW, Stucker B. "Additive manufacturing technologies: rapid prototyping to direct digital manufacturing". US: Springer; 2010. https://doi.org/ 10.1007/978-1-4419-1120-9.
35. Hehr A, Dapino MJ. "Dynamics of ultrasonic additive manufacturing". *Ultrasonics* 2017; 73:49–66.
36. Calvert, "Microstructure and Mechanical Properties of WE43 Alloy Produced Via Additive Friction Stir Technology", *J. of Manf. Techn*. 2015 Elsevier
37. Akash Mukhopadhyay et al. "Mechanical and microstructural characterization of aluminium powder deposit made by friction stir based additive manufacturing". *Journal of Materials Processing Technology*, 2020 Elsevier
38. N. Singh, "Selective laser manufacturing of Ti-based alloys and composites: impact of process parameters, application trends, and future prospects". *Materials Today Advances*, 2020 8, 100097
39. Anne I. Mertens "Fusion-Based Additive Manufacturing for Processing Aluminum Alloys: State-of-the-Art and Challenges". *Advanced Engineering Materials*, 2017 19, Wiley
40. Hang Z, RS Mishra "Additive friction stir deposition: a deformation processing route to metal additive manufacturing", *Materials Research Letters*, 9, 2020 Taylor and Francis

41. Langelandsvik G, Akselsen OM, Furu T, et al. “Review of aluminum alloy development for wire Arc additive manufacturing”. *Materials (Basel)* 2021;14(18): 112006.
42. Rodrigues TA, Duarte V, Miranda RM, et al. “Current status and perspectives on wire and Arc additive manufacturing (WAAM)”. *Materials (Basel)*, 2019 ;12(7).
43. Karayel E, Bozkurt Y. “Additive manufacturing method and different welding Applications”. *J Mater Res Technol*, 2020 ;9(5):11424–38.
44. Jin W, Zhang C, Jin S, et al. “Wire Arc additive manufacturing of stainless steels: a Review”. *Appl Sci*, 2020, ;10(5):1563.
45. D. Ding, Z. Pan, D. Cuiuri, H. Li, Int. J. Adv. Manuf. Technol. 81, 2015, 465–481.
46. S.W. Williams, F. Martina, A.C. Addison, J. Ding, G. Pardal, P. Colegrove, *Mater. Sci. Tech.-Lond*. 32, 2016, 641–647.
47. F. Wang, S. Williams, P. Colegrove, A.A. Antonysamy, *Metall. Mater. Trans.* A 44, 2013, 968–977.
48. Z. Pan, D. Ding, B. Wu, D. Cuiuri, H. Li, J. Norrish, “Arc welding processes for additive manufacturing: a review”, *Transactions on Intelligent Welding Manufacturing*, Volume I No. 1 Springer, Singapore, Singapore, 2018, pp. 3–24.
49. Thapliyal S. “Challenges associated with the wire arc additive manufacturing (WAAM) of aluminum alloys”. *Mater Res Express*, 2019 ;6(11).
50. Gu J, Ding J, Williams SW, et al. “The effect of inter-layer cold working and post deposition heat treatment on porosity in additively manufactured aluminum alloys”. *J Mater Process Technol* 2016; 230:26–34.
51. Horgar A, Fostervoll H, Nyhus B, et al. “Additive manufacturing using WAAM with AA5183 wire”. *J Mater Process Technol* 2018; 259:68–74.
52. Santos Souza ER, Weber RP, Monteiro SN, et al. “Microstructure effect of heat input on ballistic performance of welded high strength armor steel”. *Materials* 2021;14 (19).
53. AliI Y, Henckell P, Hildebrand J, et al. “Wire arc additive manufacturing of hot work tool steel with CMT process”. *J Mater Process Technol* 2019; 269:109–16.
54. Ma Y, Yang Y, Jia X, et al. “Effect of welding heat input on microstructure and properties of coarse-grained HAZ of 500 MPa high-strength low-alloy steel”. *Trans Indian Inst Met* 2022; 75 (7):1877–84.
55. Rodrigues TA, Duarte V, Avila JA, et al. “Wire and arc additive manufacturing of HSLA steel: effect of thermal cycles on microstructure and mechanical properties”. *Addit Manuf* 2019; 27:440–50.
56. Caballero A, Ding J, Ganguly S, et al. “Wire + Arc additive manufacture of 17-4 PH stainless steel: effect of different processing conditions on microstructure, hardness, and tensile strength”. *J Mater Process Technol* 2019; 268:54–62.

57. Wang L, Xue J, Wang Q. “Correlation between arc mode, microstructure, and mechanical properties during wire arc additive manufacturing of 316L stainless steel”. *Mater Sci Eng A Struct Mater* 2019; 751:183–90.
58. Hackenhaar W, Mazzaferro JAE, Montevecchi F, et al. “An experimental-numerical study of active cooling in wire arc additive manufacturing”. J Manuf Processes 2020; 52:58–65.
59. Piscopo G, Iuliano L. “Current research and industrial application of laser powder directed energy deposition”. *Int J Adv Manuf Technol* 2022:1–25. https://doi.org/ 10.1007/s00170-021-08596-w.
60. Tepylo N, Huang X, Patnaik PC. “Laser-based additive manufacturing technologies for aerospace applications”. *Adv Eng Mater* 2019;21. https://doi.org/10.1002/ adem.201900617.
61. Vafadar A, Guzzomi F, Rassau A, Hayward K. “Advances in metal additive manufacturing: a review of common processes, industrial applications, and current challenges”. *Appl Sci* 2021; 11:1–33. https://doi.org/10.3390/ app11031213.
62. Bouaziz MA, Djouda JM, Kauffmann J, Hild F. “Microscale mechanical characterization of 17-4PH stainless steel fabricated by atomic diffusion additive manufacturing (ADAM)”. In: *Procedia Struct. Integr*. Elsevier B.V.; 2020. p. 1039–46. https://doi.org/10.1016/j.prostr.2020.11.119.
63. Bhaskar Dutta, “Directed Energy Deposition (DED) Technology”, Editor(s): Francisca G. Caballero, *Encyclopedia of Materials: Metals and Alloys*, Elsevier, 2022, Pages 66-84, ISBN 9780128197332, https://doi.org/10.1016/B978-0-12-819726-4.00035-1
64. Carroll BE, Palmer TA, Beese AM. “Anisotropic tensile behavior of ti-6Al-4V components fabricated with directed energy deposition additive manufacturing”. *Acta Mater* 2015; 87:309–20. https://doi.org/10.1016/j.actamat.2014.12.054
65. Rodríguez-González, P.; Ruiz-Navas, E.M.; Gordo, E. “Wire Arc Additive Manufacturing (WAAM) for Aluminum-Lithium Alloys: A Review”. *Materials* 2023, 16, 1375. https://doi.org/10.3390/ma16041375
66. Xia C, Pan Z, Polden J, et al. “A review on wire arc additive manufacturing: Monitoring, control and a framework of automated system”. *J Manuf Syst* 2020;57: 31–45.
67. Bai X, Colegrove P, Ding J, et al. “Numerical analysis of heat transfer and fluid flow in multilayer deposition of PAW-based wire and arc additive manufacturing”. *Int J Heat Mass Transfer* 2018; 124:504–16.
68. Rosli NA, Alkahari MR, Abdollah MFB, et al. “Review on effect of heat input for wire arc additive manufacturing process*”. J Mater Res Technol* 2021; 11:2127–45.
69. Raut LP, Taiwade RV. “Wire arc additive manufacturing: a comprehensive review and research directions”. *J Mater Eng Perform* 2021 ;30(7):4768–91.

70. Barath Kumar MD, Manikandan M. “Assessment of process, parameters, residual stress mitigation, post treatments and finite element analysis simulations of wire arc additive manufacturing technique”. *Met Mater Int* 2021 ;28(1):54–111.
71. Kou, S. Welding Metallurgy; Cambridge University Press: New York, NY, USA, 2003.
72. Song, Y.B.; Li, L.; Lu, S.M.; Yan, A.; Zhou, D.J. “Research status and perspective of 7xxx series aluminum alloys welding”. *Chin. J. Nonferrous Met*. 2018, 28, 10.
73. Peng, X.Y.; Cao, X.W.; Duan, Y.L. “Microstructures and properties of MIG welded joint of 7020 aluminum alloy”. *Chin. J. Nonferrous Met*. 2014, 24, 912–918.
74. Wang, J.; Chen, X.; Yang, L.; Zhang, G. “Sequentially combined thermo-mechanical and mechanical simulation of double-pulse MIG welding of 6061-T6 aluminum alloy sheets”. J. *Manuf. Process.* 2022, 77, 616–631.
75. K. Liu, X. Chen, Q. Shen, Z. Pan, R.A. Singh, S. Jayalakshmi, S. Konovalov, “Microstructural evolution and mechanical properties of deep cryogenic treated Cu–Al–Si alloy fabricated by cold metal transfer (CMT) process”, *Mater. Charact*. 2019, https://doi.org/10.1016/j. matchar.2019.110011.
76. Liqiong, L.I.; Jin, C. “Numerical simulation of hot cracking of 7075 Al alloy by plasma-MIG hybrid welded joint”. *Electr. Weld. Mach*. 2019, 49, 95–100.
77. Stopyra, W.; Gruber, K.; Smolina, I.; Kurzynowski, T.; Ku ´znicka, B. “Laser powder bed fusion of AA7075 alloy: Influence of process parameters on porosity and hot cracking”. *Addit. Manuf.* 2020, 35, 101270. [CrossRef]
78. Huang, L.; Chen, X.; Konovalov, S.; Siddiquee, A.N.; Lu, G.; Pan, X. “The Effect of Wire Feeding Speed on Solidification Cracking of CMT Welding for Al-Si Alloys”. *Metals* 2021, 11, 267.
79. Soysal, T.; Kou, S. “A Simple Test for Solidification Cracking Susceptibility and Filler Metal Effect”. *Weld*. J. 2017, 96, 389S–401S.
80. A. Rajesh Kannan, N. Siva Shanmugam, Yasam Palguna, B. Girinath, Wonjoo Lee, Jonghun Yoon, “Effect of double-side welding on the microstructural characteristics and mechanical performance of dissimilar AA6061-AA5052 aluminium alloys”, *Materials Letters*, Volume 331, 2023, 133444, ISSN 0167-577X, https://doi.org/10.1016/j.matlet.2022.133444.
81. S.S. Sravanthia, Swati Ghosh Acharyya, Praveen Chapala, “Effect of GMAW brazing and cold metal transfer welding techniques on the corrosion behaviour of aluminium-steel lap joints”, *Mater. Today: Proc*. 18, 2019. 2708–2716.
82. A. Rajesh Kannan, N. Siva Shanmugam, S. Naveen Kumar, “Effect of Arc length correction on weld bead geometry and mechanical properties of AISI 316Lweldments by cold metal transfer (CMT) process”, *Mater. Today: Proc*. 18, 2019, 3916–3921.
83. R. Rajeshkumar, K. Devakumaran, Kumkum Banerjee, “Role of interfacial microstructure on mechanical properties of cold metal transfer welded dissimilar A6061-T6 and A6082-T6

joints", *Materials Letters*, Volume 279, 2020, 128521, ISSN 0167-577X, https://doi.org/10.1016/j.matlet.2020.128521.

84. Zhang, H., Feng, J., He, P., Zhang, B., Chen, J., & Wang, L. "The arc characteristics and metal transfer behaviour of cold metal transfer and its use in joining aluminium to zinc-coated steel. - structural Materials Properties Microstructure and Processing", *Materials Science and Engineering A* 2009, 499, 111-113.
85. Jie Pang, Shengsun Hu, Junqi Shen, Peng Wang, Ying Liang, "Arc characteristics and metal transfer behavior of CMT+P welding process", *Journal of Materials Processing Technology*, Volume 238, 2016,Pages 212-217,ISSN 0924-0136, https://doi.org/10.1016/j.jmatprotec.2016.07.033.
86. Jicai Feng, Hongtao Zhang, Peng He, "The CMT short-circuiting metal transfer process and its use in thin aluminium sheets welding", *Materials & Design*, Volume 30, Issue 5, 2009, Pages 1850-1852, ISSN 0261-3069, https://doi.org/10.1016/j.matdes.2008.07.015.
87. S. Selvi, A. Vishvaksenan, E. Rajasekar, "Cold metal transfer (CMT) technology - An overview", *Defence Technology*, Volume 14, Issue 1, 2018, Pages 28-44, ISSN 2214-9147, https://doi.org/10.1016/j.dt.2017.08.002.
88. Scotti, F.M.; Teixeira, F.R.; da Silva, L.J.; de Araujo, D.B.; Reis, R.P.; Scotti, "A. Thermal management in WAAM through the CMT Advanced process and an active cooling technique". *J. Manuf. Process*. 2020, 57, 23–35.
89. G.P. Rajeev, M. Kamaraj, Srinivasa R. Bakshi, "Comparison of microstructure, dilution and wear behaviour of Stellite 21 hard facing on H13 steel using cold metal transfer and plasma transferred arc welding processes", *Surf. Coat. Technol*. 375, 2019 383–394.
90. Mezrag, B.; Deschaux-Beaume, F.; Benachour, M. "Control of mass and heat transfer for steel/aluminium joining using Cold Metal Transfer process". *Sci. Technol. Weld. Join.* 2015, 20, 189–198
91. Cadiou, S.; Courtois, M.; Carin, M.; Berckmans, W. "3D heat transfer, fluid flow and electromagnetic model for cold metal transfer wire arc additive manufacturing (CMT-WAAM)". *Addit. Manuf.* 2020, 36, 101541.
92. Su C, Chen X, Gao C, et al. "Effect of heat input on microstructure and mechanical properties of Al-Mg alloys fabricated by WAAM". *Appl Surf Sci* 2019; 486:431–40.
93. Jafari D, Vaneker THJ, Gibson I. "Wire and arc additive manufacturing: Opportunities and challenges to control the quality and accuracy of manufactured parts". *Mater Des* 2021; 202:109471.
94. Wang D, Lu J, Tang S, et al. "Reducing porosity and refining grains for Arc additive manufacturing aluminum alloy by adjusting Arc pulse frequency and current". *Materials (Basel)* 2018;11(8):1344.

95. Zhao Y, Jia Y, Chen S, et al. “Process planning strategy for wire-arc additive manufacturing: thermal behavior considerations”. *Addit Manuf* 2020; 32:100935.
96. Guo Y, Han Q, Hu J, et al. “Comparative study on Wire-Arc additive manufacturing and conventional casting of Al-Si alloys: porosity, microstructure and mechanical property”. *Acta Metallur Sinica-English Lett* 2022;35(3):475–85.
97. Derekar KS. “A review of wire arc additive manufacturing and advances in wire arc additive manufacturing of aluminium”. *Mater Sci Technol* 2018;34(8):895–916.
98. Zhou Y, Lin X, Kang N, et al. “Influence of travel speed on microstructure and mechanical properties of wire + arc additively manufactured 2219 aluminum alloy”. J *Mater Sci Mater Med* 2020; 37:143–53.
99. Wang, N.; Mokadem, S.; Rappaz, M.; Kurz, W. “Solidification cracking of superalloy single- and bi-crystals”. *Acta Mater*. 2004, 52, 3173–3182.
100. Liu, J.; Zeng, P.; Wu, Y.; Kou, S. “Determination of tensile strain causing solidification cracking in welding”. *Sci. Technol. Weld. Join*. 2020, 25, 431–437.
101. G.P. Rajeev, M. Kamaraj, Srinivasa R. Bakshi, “Hard facing of AISI H13 tool steel with Satellite 21 alloy using cold metal transfer welding process”, *Surf. Coat. Technol*. 2017, https://doi.org/10.1016/j.surfcoat.2017.07.050.
102. G.P. Rajeev, M. Kamaraj, Srinivasa R. Bakshi, “Comparison of microstructure, dilution and wear behaviour of Stellite 21 hard facing on H13 steel using cold metal transfer and plasma transferred arc welding processes”, *Surf. Coat. Technol.* 375, 2019, 383–394.
103. Beyrullah Gungor, Erdinc Kaluc, Emel Taban, S.I.K. Aydin, “Mechanical and microstructural properties of robotic cold metal transfer (CMT) welded 5083– H111 and 6082–T651 aluminum alloys”, *Mater. Des.* 54, 2014, 207–211.
104. L. Guojin, Z. Peilei, W. Xi, N. Yunpeng, Y. Zhishui, Y. Hua, L. Qinghua, “Gap bridging of 6061 aluminum alloy joints welded by variable polarity cold metal transfer”, *J. Mater. Process. Technol.* 2010, https://doi.org/10.1016/j. jmatprotec.2018.01.004.
105. Chen Zhang, Yufei Li, Ming Gao, Xiaoyan Zeng, “Wire arc additive manufacturing of Al-6Mgalloy using variable polarity cold metal transfer arc as power source”, *Mater. Sci. Eng., A* 711, 2018, 415–423.
106. Jian Gou, Junqi Shen, Hu Shengsun, Yinbao Tian, Ying Liang, “Microstructure and mechanical properties of as- built and heat-treated Ti6Al-4V alloy prepared by cold metal transfer additive manufacturing”, *J. Manuf. Processes* 42,2019 41–50.
107. Yinbao Tian, Junqi Shen, Shengsun Hu, Ying Liang, Pengfei Bai, “Effects of ultrasonic peening treatment on surface quality of CMT-welds of Al alloys”, *Journal of Materials Processing Technology*, Volume 254, 2018, Pages 193-200, ISSN 0924-0136, https://doi.org/10.1016/j.jmatprotec.2017.11.029.

108. N. Pavan Kumar, S. Arungalai Vendan, N. Siva, Shanmugam, “Investigations on the parametric effects of cold metal transfer process on the microstructural aspects in AA6061”, *J. Alloy. Compd*. (2015), https://doi.org/10.1016/ j.jallcom.2015.10.166.
109. Cong, B., Ding, J. & Williams, S. “Effect of arc mode in cold metal transfer process on porosity of additively manufactured Al-6.3%Cu alloy*”. Int J Adv Manuf Technol* 76, 1593–1606 2015. https://doi.org/10.1007/s00170-014-6346-x
110. Chen Zhang, Yufei Li, Ming Gao, Xiaoyan Zeng, “Wire arc additive manufacturing of Al-6Mg alloy using variable polarity cold metal transfer arc as power source”, *Materials Science and Engineering: A*, Volume 711, 2018, Pages 415-423, ISSN 0921-5093, https://doi.org/10.1016/j.msea.2017.
111. Sen Li, Lin-Jie Zhang, Jie Ning, Xiang Wang, Gui-Feng Zhang, Jian-Xun Zhang, Suck-Joo Na, Bodaghi Fatemeh, “Comparative study on the microstructures and properties of wire+arc additively manufactured 5356 aluminium alloy with argon and nitrogen as the shielding gas”, *Additive Manufacturing*, Volume 34, 2020, 101206, ISSN 2214-8604, https://doi.org/10.1016/j.addma.2020.101206.
112. Siyu Zhou, Ke Wu, Guang Yang, Bin Wu, Lanyun Qin, Hao Wu, Chaoyue Yang, “Microstructure and mechanical properties of wire arc additively manufactured 205A high strength aluminum alloy: The comparison of as-deposited and T6 heat-treated samples”, *Materials Characterization*, Volume 189, 2022,111990, ISSN 1044-5803,https://doi.org/10.1016/j.matchar.2022.111990.
113. Shujun Chen, Min Xu, Tao Yuan, Xiaoqing Jiang, Hongda Zhang, Xing Zheng, “Thermal–microstructural analysis of the mechanism of liquation cracks in wire-arc additive manufacturing of Al–Zn–Mg–Cu alloy”, *Journal of Materials Research and Technology*, Volume 16, 2022, Pages 1260-1271, ISSN 2238-7854, https://doi.org/10.1016/j.jmrt.2021.12.016.
114. Zhanliang Yu, Tao Yuan, Min Xu, Hongda Zhang, Xiaoqing Jiang, Shujun Chen, “Microstructure and mechanical properties of Al-Zn-Mg-Cu alloy fabricated by wire + arc additive manufacturing”, *Journal of Manufacturing Processes*, Volume 62, 2021, Pages 430-439,ISSN 1526-6125, https://doi.org/10.1016/j.jmapro.2020.12.045.
115. Xinpeng Guo, Huijun Li, Peng Xue, Zengxi Pan, Rongzheng Xu, Dingrui Ni, Zongyi Ma, “Microstructure and mechanical properties of 600 MPa grade ultra-high strength aluminum alloy fabricated by wire-arc additive manufacturing”, *Journal of Materials Science & Technology*, Volume 149, 2023, Pages 56-66, ISSN 1005-0302, https://doi.org/10.1016/j.jmst.2022.12.007.
116. Pramod, R., Kumar, S. M., Girinath, B., Kannan, A. R., Kumar, N. P., & Shanmugam, N. S. “Fabrication, characterisation, and finite element analysis of cold metal transfer–based wire and arc additive–manufactured aluminium alloy 4043 cylinder”. *Welding in the World*, 2020. 64, 1905-1919.

117. Nandagopal, K., & Kailasanathan, C. “Analysis of mechanical properties and optimization of gas tungsten Arc welding (GTAW) parameters on dissimilar metal titanium (6Al4V) and aluminium 7075 by Taguchi and ANOVA techniques”. *Journal of Alloys and Compounds*, 2016. 682, 503-516.
118. Sambasiva Rao, A., Madhusudhan Reddy, G., & Prasad, K. S “Microstructure and tensile properties of dissimilar metal gas tungsten arc welding of aluminium to titanium alloy”. *Materials Science and Technology*, 2011, 27(1), 65-70.
119. Ahmad, I., & Arya, S. “To Study the Micro-Structural of Aluminum Alloy AA-6061 Welded Using TIG Welding Process at Different Welding Current”. *Int. Res. J. Eng. Technol*, 2018. 5, 395-403.
120. Yang, G., Ma, J., Wang, H. P., Carlson, B., & Kovacevic, R. “Studying the effect of lubricant on laser joining of AA 6111 panels with the addition of AA 4047 filler wire”. *Materials & Design*, 2017. 116, 176-187.
121. Yang, G., Ma, J., Carlson, B., Wang, H. P., & Kovacevic, R. “Effect of laser beam configuration on microstructure evolution and joint performance in laser joining AA 6111 panels”. *Materials & Design*, 2017. 123, 197-210.
122. Mathieu, A., Pontevicci, S., Viala, J. C., Cicala, E., Matteï, S., & Grevey, D. “Laser brazing of a steel/aluminium assembly with hot filler wire (88% Al, 12% Si)”. *Materials Science and Engineering: A*, 2006, 435, 19-28.
123. Babu, S., Panigrahi, S. K., Ram, G. J., Venkitakrishnan, P. V., & Kumar, R. S. “Cold metal transfer welding of aluminium alloy AA 2219 to austenitic stainless steel AISI 321” *Journal of Materials Processing Technology*, 2019, 266, 155-164.
124. Arturo Gomez Ortega, Luis Corona Galvan, Mehdi Salem, Kamel Moussaoui, Stephane Segonds, Sébastien Rouquette & Frédéric Deschaux-Beaume 2019 “Characterisation of 4043 aluminium alloy deposits obtained by wire and arc additive manufacturing using a Cold Metal Transfer process*”, Science and Technology of Welding and Joining*, 24:6, 538-547, DOI: 10.1080/13621718.2018.1564986
125. Vishakha Shukla, Vikash Kumar, Ankit Dixit, “Microstructural characteristics and tensile properties of ER70S-6 manufactured by Robotic CMT wire-and-arc additive manufacturing”, *Materials Today: Proceedings*, 2023, ISSN 2214-7853, https://doi.org/10.1016/j.matpr.2023.02.011.
126. Zhou S, Xie H, Ni J, Yang G, Qin L, Guo X. “Metal transfer behavior during CMT-based Wire Arc Additive Manufacturing of Ti-6Al-4V alloy”. *Journal of Manufacturing Processes.* 2022 Oct 1; 82:159-73.
127. Qi, K., Li, R., Hu, Z. et al. “Forming Appearance Analysis of 2205 Duplex Stainless Steel Fabricated by Cold Metal Transfer (CMT) Based Wire and Arc Additive Manufacture

(WAAM) Process". *J. of Materi Eng and Perform* 31, 4631–4641 2022. https://doi.org/10.1007/s11665-022-06587-w

128. Koli, Y., Arora, S., Ahmad, S. et al. "Investigations and Multi-Response Optimization of Wire Arc Additive Manufacturing Cold Metal Transfer Process Parameters for Fabrication of SS308L Samples". *J. of Materi Eng and Perform* 32, 2463–2475 2023. https://doi.org/10.1007/s11665-022-07282-6
129. Koli, Y., Yuvaraj, N., & Aravindan, S "Multi-response mathematical modeling for prediction of weld bead geometry of AA6061-T6 using response surface methodology". *Transactions of the Indian Institute of Metals*, 2020. 73, 645-666.
130. Koli, Y., Yuvaraj, N., & Aravindan, S. "Multi-response mathematical model for optimization of process parameters in CMT welding of dissimilar thickness AA6061-T6 and AA6082-T6 alloys using RSM-GRA coupled with PCA". *Advances in Industrial and Manufacturing Engineering*, 2021. 2, 100050.
131. Wu B, Ding D, Pan Z, Cuiuri D, Li H, Han J, Fei Z. "Effects of heat accumulation on the arc characteristics and metal transfer behavior in Wire Arc Additive Manufacturing of Ti6Al4V". *Journal of Materials Processing Technology*. 2017 Dec 1; 250:304-12.
132. Chen F, Yang Y, Feng H. "Regional Control and Optimization of Heat Input during CMT by Wire Arc Additive Manufacturing: Modeling and Microstructure Effects". *Materials*. 2021; 14(5):1061. https://doi.org/10.3390/ma14051061
133. Teixeira, F.R., Scotti, F.M., Jorge, V.L. et al. "Combined effect of the interlayer temperature with travel speed on features of thin wall WAAM under two cooling approaches*". Int J Adv Manuf Technol* 126, 273–289 2023. https://doi.org/10.1007/s00170-023-11105-w
134. Filippov A, Utyaganova V, Shamarin N, Vorontsov A, Savchenko N, Gurianov D, Chumaevskii A, Rubtsov V, Kolubaev E, Tarasov S. "Microstructure and corrosion resistance of AA4047/AA7075 transition zone formed using electron beam wire-feed additive manufacturing". *Materials*. 2021 Nov 16;14(22):6931
135. Chen C, Sun G, Du W, Liu J, Zhang H. "Effect of equivalent heat input on WAAM Al-Si alloy". *International Journal of Mechanical Sciences*. 2023 Jan 15; 238:107831.
136. Montgomery DC. "Design and analysis of experiments". John wiley & sons; 2017.
137. Ren G, Heo S, Kim TH, Cheong C. "Response surface method-based optimization of the shroud of an axial cooling fan for high performance and low noise". *Journal of Mechanical Science and Technology*. 2013 Jan; 27:33-42.
138. Guang Yang, Junjie Ma, Hui-Ping Wang, Blair Carlson, Radovan Kovacevic, "Studying the effect of lubricant on laser joining of AA 6111 panels with the addition of AA 4047 filler wire", *Materials & Design*, Volume 116, Pages 176-187, ISSN 0264-1275, https://doi.org/10.1016/j.matdes.2016.12.014.

139. Gomez Ortega A, Corona Galvan L, Deschaux-Beaume F, Mezrag B, Rouquette S. “Effect of process parameters on the quality of aluminium alloy Al5Si deposits in wire and arc additive manufacturing using a cold metal transfer processs”. *Science and Technology of Welding and Joining*. 2018 May 19;23(4):316-32.
140. Tanzila Sharker, Kenneth R. Simonsen, Lucia Margheritini, Sergey V. Kucheryavskiy, Morten E. Simonsen, “Optimisation of electrochemical deposition of calcareous material during cathodic protection by implementing response surface methodology (RSM)”, *Electrochimica Acta*, Volume 444,2023,141960, ISSN 0013-4686, https://doi.org/10.1016/j.electacta.2023.141960.
141. Achara Taweesan, Thongchai Kanabkaew, Nawatch Surinkul, Chongrak Polprasert, “Convenient solutions to inconvenient truth: Domestic wastewater management-based approaches to sustainable development goal no. 6”, *Environmental and Sustainability Indicators*, Volume 18,2023,100255, ISSN 2665-9727, https://doi.org/10.1016/j.indic.2023.100255.
142. Ren, Guangzhi & Heo, Seung & Kim, Tae-Hoon & Cheong, Cheolung. ‘Response surface method-based optimization of the shroud of an axial cooling fan for high performance and low noise”. *Journal of Mechanical Science and Technology*. 2013. 27. 10.1007/s12206-012-1220-y.
143. Novelino AL, Carvalho GC, Ziberov M. “Influence of WAAM-CMT deposition parameters on wall geometry”. *Advances in Industrial and Manufacturing Engineering.* 2022 Nov 1; 5:100105.
144. Chen C, Sun G, Du W, Liu J, Zhang H. “Effect of equivalent heat input on WAAM Al-Si alloy. International” *Journal of Mechanical Sciences*. 2023 Jan 15; 238:107831.
145. Koli Y, Yuvaraj N, Sivanandam A, Vipin. “Control of humping phenomenon and analyzing mechanical properties of Al–Si wire-arc additive manufacturing fabricated samples using cold metal transfer process”. *Proceedings of the Institution of Mechanical Engineers, Part C: Journal of Mechanical Engineering Science*. 2022 Jan;236(2):984-96.
146. Wieczorowski M, Pereira A, Carou D, Gapinski B, Ramírez I. “Characterization of 5356 Aluminum Walls Produced by Wire Arc Additive Manufacturing (WAAM)”. *Materials.* 2023 Mar 23;16(7):2570.
147. Yuan L, Pan Z, Ding D, et al. “Investigation of humping phenomenon for the multi-directional robotic wire and arc additive manufacturing”. *Robot Cim-Int Manuf* 2020; 63: 101916
148. Teixeira, F.R., Scotti, F.M., Vilarinho, L.O. et al. “Transferability of the working envelope approach for parameter selection and optimization in thin wall WAAM”. *Int J Adv Manuf Technol* 119, 969–989 2022. https://doi.org/10.1007/s00170-021-08326-2
149. Wu D, Hua X, Ye D, et al. “Understanding of humping formation and suppression mechanisms using the numerical simulation”. *Int J Heat Mass Tran* 2017; 104: 634–643.

150. Ragavendran M, Chandrasekhar N, Ravikumar R, Saxena R, Vasudevan M, Bhaduri AK. "Optimization of hybrid laser–TIG welding of 316LN steel using response surface methodology (RSM)". *Optics and Lasers in Engineering*. 2017 Jul 1; 94:27-36.
151. Elemary BR. "Evaluation and improvement of promising rubber recycling OT machine using fractional factorial and response surface design". *Communications in Statistics: Case Studies, Data Analysis and Applications.* 2019 Jul 3;5(3):168-88.
152. Goyal H, Mandal N, Roy H, Mitra SK, Mondal B. "Multi response optimization for processing Al–SiCp composites: an approach towards enhancement of mechanical properties". *Transactions of the Indian Institute of Metals*. 2015 Jun; 68:453-63.
153. Q. Miao, D. Wu, D. Chai, Y. Zhan, G. Bi, F. Niu, G. Ma, *Mater. Des*. 186, 108205, 2020
154. Guo Y, Han Q, Hu J, Yang X, Mao P, Wang J, Sun S, He Z, Lu J, Liu C. "Comparative Study on Wire-Arc Additive Manufacturing and Conventional Casting of Al–Si Alloys: Porosity, Microstructure and Mechanical Property". *Acta Metallurgica Sinica (English Letters).* 2022:1-1.
155. Kisarev AV, Kobernik NV. "Study on formation of aluminum alloy thin wall produced with WAAM method under various thermal conditions". In *IOP Conference Series: Materials Science and Engineering* 2020 Feb 1 (Vol. 759, No. 1, p. 012014). IOP Publishing.
156. Athaib NH, Haleem AH, Al-Zubaidy B. "A review of Wire Arc Additive Manufacturing (WAAM) of Aluminium Composite, Process, Classification, Advantages, Challenges, and Application". In *Journal of Physics: Conference Series* 2021 Aug 1 (Vol. 1973, No. 1, p. 012083). IOP Publishing.
157. Pramod, R., Kumar, S.M., Girinath, B. et al. "Fabrication, characterisation, and finite element analysis of cold metal transfer–based wire and arc additive–manufactured aluminium alloy 4043 cylinder'. *Weld World* 64, 1905–1919, 2020. https://doi.org/10.1007/s40194-020-00970-8
158. Keist, J.S.; Palmer, T.A. "Development of strength-hardness relationships in additively manufactured titanium alloys". *Mater. Sci. Eng. A* 2017, 693, 214–224.
159. Hauser T, Reisch RT, Breese PP, Lutz BS, Pantano M, Nalam Y, Bela K, Kamps T, Volpp J, Kaplan AF. "Porosity in wire arc additive manufacturing of aluminium alloys". *Additive Manufacturing*, 2021 May 1; 41:101993.
160. Gierth M, Henckell P, Ali Y, Scholl J, Bergmann JP. "Wire arc additive manufacturing (WAAM) of aluminum alloy AlMg5Mn with energy-reduced gas metal arc welding (GMAW)". *Materials*. 2020 Jun 12;13(12):2671.
161. Jiangang P, Bo Y, Jinguo G, Liang Z, Hao L. "Influence of arc mode on the microstructure and mechanical properties of 5356 aluminum alloy fabricated by wire arc additive manufacturing". *Journal of Materials Research and Technology*. 2022 Sep 1; 20:1893-907.

162. Arana, Maider, Eneko Ukar, Iker Rodriguez, Amaia Iturrioz, and Pedro Alvarez.. "Strategies to Reduce Porosity in Al-Mg WAAM Parts and Their Impact on Mechanical Properties" *Metals* 11, 2021, no. 3: 524. https://doi.org/10.3390/met11030524